QUANTUM EFFECTS IN DILUTE ADSORPTION SYSTEMS

by

THOMAS BERNARD MACRURY

B.Sc., University of British Columbia, 1965

A THESIS SUBMITTED IN PARTIAL FULFILMENT OF

THE REQUIREMENTS FOR THE DEGREE OF

MASTERS OF SCIENCE

in the Department

of

Chemistry

We accept this thesis as conforming to the

required standard

THE UNIVERSITY OF BRITISH COLUMBIA

September, 1967

In presenting this thesis in partial fulfilment of the requirements for an advanced degree at the University of British Columbia, I agree that the Library shall make it freely available for reference and Study. I further agree that permission for extensive copying of this thesis for scholarly purposes may be granted by the Head of my Department or by his representatives. It is understood that copying or publication of this thesis for financial gain shall not be allowed without my written permission.

Department of Chemistry

The University of British Columbia
Vancouver 8, Canada

Date Sept. 11 /67

ABSTRACT

The adsorption isotherm and the equation of state for the two-dimensional gas are derived from the grand canonical ensemble. Then the quantum statistical equation of state is developed and applied to the two-dimensional second virial coefficient, $B^{(2)}$, and the second gas-surface virial coefficient, B_{AS}. We compare theoretically the (12,6) and (12,6,3) potential models for $B^{(2)}$. Finally the adsorption data for CH_4, CD_4, H_2 and D_2 on graphite are analysed quantally for the two-dimensional second virial coefficient and the second gas-surface virial coefficient.

ACKNOWLEDGEMENT

I am sincerely grateful to Dr. J.R. Sams Jr. for his patience and invaluable guidance during the course of this work. I would also like to thank R. Wolfe for his assistance in some of the computer programming.

TABLE OF CONTENTS

	Page
ABSTRACT	
ACKNOWLEDGEMENT	i
LIST OF TABLES	ii
LIST OF FIGURES	iv
CHAPTER 1. Introduction	v
CHAPTER 2. The Adsorption Isotherm and the Equation of State	
Three-dimensional developement	11
Two-dimensional development	14
CHAPTER 3. Quantum Statistical Equation of State	
General development	20
Two-dimensional second virial coefficient	26
Second gas-surface virial coefficient	31
CHAPTER 4. Theoretical Comparison of the (12,6) and (12,6,3) Models for $B^{(2)*}$	35
CHAPTER 5. Analysis of the Data	
Two-dimensional second virial coefficient	43
Second gas-surface virial coefficient	50
APPENDIX 1	57
APPENDIX 2	63
BIBLIOGRAPHY	64

LIST OF TABLES

Table		Page
I	Curve fit results for two-dimensional CH_4 and CD_4 on graphite.	45a
II	Values of Δ and δ for CH_4 and CD_4 based on the four models.	46a
III	B_{AS} and C_{AAS} data for H_2 and D_2.	48a
IV	Curve fit results for two-dimensional (12,6) H_2 and D_2 on graphite.	49a
V	Values of Δ and δ for two-dimensional (12,6) H_2 and D_2.	50a
VI	Classical and Quantum Kirkwood-Muller fit results for CH_4, CD_4, H_2 and D_2.	53a
VII	Quantum Slater-Kirkwood and London fit results for CH_4, CD_4, H_2 and D_2.	53b
VIII	Values of $B_{CI}^{(2)*}$, $B_{I}^{(2)*}$, and $B_{II}^{(2)*}$ at selected values of T^* and η for the (12,6,3) potential function.	57
IX	Values of B_{AS}^{II*} for the (9,3), (10,4) and (12,3) models.	63

LIST OF FIGURES

Figure		Page
1.	Curves of reduced two-dimensional second virial coefficient versus reduced temperature.	35a
2.	Curves of reduced two-dimensional second virial coefficient versus relative reduced temperature.	36a
3.	Radius of convergence curves.	38a
4.	Quantum (12,6,3) curves for different n values.	39a
5.	Curves of the second virial coefficient in one, two, and three dimensions.	40a

CHAPTER I

INTRODUCTION

Before 1954, nearly all adsorption data were taken below the critical temperature of the adsorbate. Lateral interactions, multilayer formation, and possible capillary condensation are important in this region and since the theory of these phenomena is even more complex than the theory of liquids, it seemed advantageous to investigate adsorption at higher temperatures. Steele and Halsey[1] found that if the temperature was high enough and the gas pressure low, the interactions between adsorbate molecules could be ignored and the problem of the interaction of single molecules with the surface investigated.

The adsorption isotherm was expanded in a virial series, analogous to that used in imperfect gas theory. The leading term in the expansion gives the Henry's law constant of the isotherm. At somewhat lower temperatures and higher pressures, additional terms, which account for interactions between the admolecules, must be included. An exact derivation in the classical grand canonical ensemble[2] leads to a development of the isotherm, expressing the number of molecules adsorbed at Kelvin temperature T and bulk gas pressure p, in terms of the irreducible cluster integrals:

$$\bar{N}a = \beta_1 \left(\frac{P}{kT}\right) + \left(\beta_2 + \frac{3}{2}\beta_1\beta_1^{\circ}\right)\left(\frac{P}{kT}\right)^2 + \ldots, \tag{1.01}$$

$$= B_{AS}\left(\frac{P}{kT}\right) + C_{AAS}\left(\frac{P}{kT}\right)^2 + \ldots, \tag{1.01a}$$

$$\beta_1 = \int f_1 d\underset{\sim}{r}_1 \quad , \quad \beta_1^{\circ} = V^{-1}\iint f_{12} d\underset{\sim}{r}_1 d\underset{\sim}{r}_2 \, , \tag{1.02}$$

$$\beta_2 = \iint f_1 f_2 f_{12} d\underset{\sim}{r}_1 d\underset{\sim}{r}_2 \, ,$$

where the f's are the usual Mayer functions,[3]

$$1+f_{ij} = \exp\left[-\beta\phi(r_{ij})\right],$$
$$1+f_{i} = \exp\left[-\beta\phi_s(\underset{\sim}{r}_i)\right]. \qquad (1.03)$$

$\phi(r_{ij})$ is the pair potential between molecules i and j, $\phi_s(\underset{\sim}{r}_i)$ the interaction potential of molecule i at $\underset{\sim}{r}_i$ with the solid, and $\beta = (kT)^{-1}$.

In this statistical mechanical development of the theory of physical adsorption, the following assumptions are required:

1. One can treat the adsorbent as an inert solid which merely furnishes a potential energy of interaction between the adsorbate molecules and the adsorbent. The interaction energy between the ith gas molecule and the adsorbent will be denoted by $\phi_s(\underset{\sim}{r}_i)$.

2. The interaction energies between molecules in the gas phase are pair-wise additive. The interaction energy between molecules i and j can be written as $\phi(\underset{\sim}{r}_i, \underset{\sim}{r}_j)$ or as $\phi(\underset{\sim}{r}_{ij}, \underset{\sim}{R}_{ij})$, where

$$\underset{\sim}{r}_{ij} = \underset{\sim}{r}_i - \underset{\sim}{r}_j,$$
$$\underset{\sim}{R}_{ij} = \underset{\sim}{r}_i + \underset{\sim}{r}_j. \qquad (1.04)$$

In many treatments, the problem can be simplified further by assuming that the potential depends on the separation between i and j molecules, ie $\phi(r_{ij})$.

3. The various interaction potentials are independent of molecular orientation. This infers that all gas molecules will have spherical symmetry, at least in the absence of the solid. Furthermore,

any changes in internal vibration state upon adsorption will be neglected. Using these assumptions, the total potential energy of N molecules in a configuration $\underset{\sim}{r}_1 \ldots \underset{\sim}{r}_N$ and interacting with each other and with a solid adsorbent is

$$\phi(\underset{\sim}{r}_1 \ldots \underset{\sim}{r}_N) = \sum_{i=1}^{N} \phi_s(\underset{\sim}{r}_i) + \sum_{1 \leq i < j \leq N} \phi(r_{ij}). \qquad (1.05)$$

It is clear from the isotherm equation (1.01a) that, when terms higher than the quadratic are neglected, plots of $\bar{N}a/p$ versus p are linear, with gradient $(C_{AAS})/(kT)^2$ and intercept B_{AS}/kT. Therefore these so-called gas-surface virial coefficients can be obtained experimentally from adsorption isotherms measured at low surface densities.

The two parameter theory derived by Steele and Halsey[1] for the second order (or Henry's Law) region of the isotherm, allowed the evaluation of the depth of the gas-surface interaction well, ε_{ls}, and the capacity factor Az_o, where A is the surface area of the adsorbent and z_o the apparent gas-solid collision diameter. From the observed ε_{ls} and any of the familiar expressions for the dispersion energy constant, one can calculate a value for z_o, and hence A. This provided a new method of determining surface areas which was independent of any multilayer adsorption theory or any molecular cross-sectional estimates.

A model for the next term in the isotherm equation, which accounts for the simultaneous interactions of two gas molecules with the surface and with each other was presented by Freeman and Halsey[4] and later refined by Freeman.[5] Employing Lennard-Jones potentials for both gas-solid and gas-gas interactions, agreement with experimental results was deemed to be

unsatisfactory. It was suggested that this might be due to the fact that the intermolecular potentials are not pairwise additive as assumed in the model. Recently it has been pointed out[6,7] that the solid has an appreciable effect on the pairwise interaction between molecules near the surface. The attractive part of the energy appeared to be enhanced by about 20% when $\underset{\sim}{r}_{ij}$ was perpendicular to the surface and decreased by approximately the same amount when $\underset{\sim}{r}_{ij}$ was parallel.

Since the evaluation of β_2 for realistic potentials is cumbersome, an alternative method of treating the data has been devised. The computations can be simplified considerably by reducing the 3N-dimensional cluster integrals in (1.02) and (1.03) to 2N-dimensional integrals in the plane normal to the field direction. Using the method of steepest descents, Steele[8] has shown that at low temperatures the two dimensional equation of state of the adsorbate is given by

$$\frac{\phi A}{\bar{N} a k T} = 1 - \left(\frac{\beta_2}{2\beta_1^2} + \frac{\beta_1^\circ}{\beta_1} \right) \bar{N}a - \ldots , \tag{1.06}$$

where ϕ is the spreading pressure. This equation has the form of a two-dimensional virial expansion in the surface density $\bar{N}a/A$,

$$\frac{\phi A}{\bar{N} a k T} = 1 + B^{(2)} \frac{\bar{N}a}{A} + \ldots , \tag{1.07}$$

where in the reduction from 3N dimensions to 2N dimensions,

$$-\left(\beta_2 + 2\beta_1 \beta_1^\circ \right) / 2\beta_1^2 \longrightarrow B^{(2)} / A. \tag{1.08}$$

$B^{(2)}$ is the two dimensional second virial coefficient and $B^{(2)}/A$ can be measured from the experimental gas-surface virial coefficients. Sams, Constabaris and Halsey[9] have applied this equation to the interaction of argon with graphitic carbon.

Correction terms to account for the motion of the molecules in the field direction can be written down as well, and one finds that under the normal experimental conditions these corrections are small and (1.08) should provide quite an accurate approximation. Thus the gas-gas-field interaction can be treated as an effective gas-gas interaction, the field serving merely to restrict the molecular motions to two dimensions.

The problem then is to specify the form of the effective two-dimensional interaction potential, since it is clearly incorrect to employ the usual gas phase potential function. Sinanoglu and Pitzer[6], and Yaris[10] have derived theoretical expressions for the three-body energy in gas-solid interaction systems. Using third-order perturbation theory, Sinanoglu and Pitzer found that the presence of the field had the effect of introducing an additional three-body term varying as the inverse third power of the molecular separation. McLachlan[11] arrived at similar conclusions using image force methods, but has also found that at large values of the separation the inverse cube dependence goes over into an inverse sixth power dependence. For a two-dimensional (monolayer) model this additional interaction is repulsive, but if the admolecules are directly above and below one another, the three-body term becomes attractive[6]. These findings have led to the use, in analysing experimental data, of two assumed forms for the effective potential.

The first of these is the intermolecular pair potential given by Sinanoglu and Pitzer[6],

$$\phi(r_{ij}) = 4\varepsilon \left[(\sigma/r_{ij})^{12} - (\sigma/r_{ij})^{6}\right] + (S/r_{ij}^{3})\,(1-3\cos^{2}\theta\,), \tag{1.09}$$

where ε and σ are the bulk-gas Lennard-Jones (12,6) potential parameters, θ the angle between r_{ij} and the surface normal, and

$$S = \alpha_1 E_{1s} \left(\Delta_o + \gamma_m \Delta_1\right)/4\,, \tag{1.10}$$

where

$$\Delta_o = (2\delta_1 + \delta_s)/(\delta_1 + \delta_s)\,, \tag{1.11}$$

$$\Delta_1 = (6\delta_1 + 7\delta_s)/(\delta_1 + \delta_s)\,, \tag{1.12}$$

$$\gamma_m = E_{es}/E_{1s}. \tag{1.13}$$

E_{1s} is the second-order perturbational energy for the interaction of a single admolecule and the surface, α_1 the polarizability of the admolecule, and δ_1 and δ_s the mean or effective excitation energies of molecular-state transitions for a single admolecule and for the surface, respectively; γ_m is the electrostatic fraction of the total second-order energy. If the two-dimensional model is applied, r_{12} becomes the two-dimensional scaler τ_{12} in a plane parallel to the surface, and $\theta = \pi/2$. Then (1.09) for the effective potential between two admolecules becomes

$$\phi_e(\tau_{12}) = 4\varepsilon \left[\tau^{*-12} - \tau^{*-6} - \eta\tau^{*-3}\right], \tag{1.14}$$

$$\tau^{*} = \tau_{12}/\sigma\,; \quad \eta = -S/4\varepsilon\sigma^{3}\,. \tag{1.15}$$

Although η can be calculated from equations (1.10) - (1.15), it has been found[12] preferable to treat it as an empirically adjustable parameter. The other potential which has been used is

$$\phi_e(\tau_{12}) = 4\varepsilon\left(\tau^{*-12} - \xi\tau^{*-6}\right), \tag{1.16}$$

where, in both potentials,

$$\tau_{12} = |\underset{\sim}{\tau}_1 - \underset{\sim}{\tau}_2|.$$

ξ is a constant which can be determined emperically by fitting experimental data to the models, and which gives a measure of the non-additivity.

Up to this point we have been concerned with the classical picture of adsorption. However, quantum effects have been measured in dilute adsorption systems and found to be of considerable importance. It has long been thought that when isotopic pairs are adsorbed on a surface, the heavier species will be adsorbed preferentially. This comes about because of the quantum statistical mass effect on the vibrational energy levels normal to the surface, with the heavier molecule lowering the energy levels slightly. This quantum effect in physical adsorption has been considered by several authors.[13,14,15] De Marcus, et,al.[13], developed the gas-surface configurational integral correct to terms of order $\hbar^2$ for a Lennard-Jones (9,3) potential, and applied the theory to data of Steele and Halsey[1] for the interaction of helium with carbon black. Freeman[15] employed the same model to interpret the adsorption of H_2 and D_2 on sugar charcoal.

In this treatment the configurational integral B_{AS} was made up of two parts, the usual classical part and the first quantum correction,

$$B_{AS} = B_{AS}^{cl} - B_{AS}^{1} \quad . \tag{1.17}$$

Both these integrals are a function of the reduced gas-surface interaction temperature ϵ_{ls}/kT, and B_{AS}^{1} is also inversely proportional to the mass.

In view of the expected increase in B_{AS} for heavier species, the results of Constabaris, Sams and Halsey[16] for the adsorption of H_2, D_2, CH_4 and CD_4 on P33 (2700°) were surprising. While D_2 had the anticipated larger excess volume than H_2, although the difference was smaller than expected, the opposite was true with the methane pair. These results can be explained by allowing for the fact that the hydrogenated and deuterated species have a slightly different internuclear distance, and thus the electronic distributions and the forces binding the electrons differ. This manifests itself in a polarizability difference between the isotopes.[17] Knaap and Beenakker have used this to explain the difference in the measured[19] gas-gas interactions of H_2 and D_2. Since dispersion forces are directly proportional to the polarizabilities of the interacting species, the percentage differences in the interaction energies from a quantum fit of the data should be commensurate with the percentage difference in the polarizabilities. Since the quantum corrections are strongly dependent upon both the depth and shape of the potential well, such a fit should provide a rather stringent test of the potential model chosen.

Yaris and Sams[20] developed the Wigner-Kirkwood expansion[21-25] to order $\hbar^4$ and examined three different models for the interaction potential,

using the data of Constabaris, et.al.[16] Due to a misprint in the $\hbar^4$ term of Uhlenbeck and Beth[21], we have recalculated the quantum corrected B_{AS} and fitted it to the data mentioned above.

The fact that significant quantum deviations were observed for gas-surface interactions suggested that it might also be possible to measure quantum effects between molecules adsorbed on a surface. To this end, the evaluation of the two-dimensional second virial coefficient in terms of the (12,6) and (12,6,3) potentials for a quantum degenerate gas at moderately high temperatures, employing the Wigner-Kirkwood expansion of the Slater sum will be considered.

In Chapter 2 of this thesis, the equation of state and the adsorption isotherm are derived through the grand-canonical ensemble. In Chapter 3, $B^{(2)}$ and B_{AS} are developed quantally for a general potential function and are evaluated numerically for certain specific potentials. Chapter 4 contains a comparison of the (12,6) and (12,6,3) models for the evaluation of $B^{(2)}$. In Chapter 5, the data[16] on the third-order interactions of H_2, D_2, CH_4, and CD_4 in the external field provided by a very uniform graphite surface P33 (2700°) are analysed. Classically both the (12,6) and (12,6,3) models have been applied[14,26,27] to the experimental data for Ar,Kr,Xe,CH_4 and CD_4. Either model led to an effective pair interaction energy which was somewhat smaller than the gas phase value. For the (12,6,3) potential, this reduction amounted to only about 8-10% of the bulk gas interaction, while for the (12,6) model the effect was approximately twice as great. Despite this difference, both models appeared to fit the data almost equally well, and it was impossible to choose between them. We hope that

the quantum treatment will provide a better test of the model. Also in Chapter 5, the B_{AS} data for H_2, D_2, CH_4 and CD_4 are analysed quantally using three different potential models in an attempt to see which model fits the data best.

CHAPTER 2

THE ADSORPTION ISOTHERM AND THE EQUATION OF STATE

If one considers a gas at given μ and T, where μ is the chemical potential, in a vessel of volume V under conditions such that the gas does not interact with the walls of the container, except to undergo perfectly elastic collisions, then the grand partition function is $\Xi^{\circ} = e^{pV/kT}$. If one considers the same gas and vessel, but now allows the gas to interact with one wall of the container, (e.g. the adsorbent) having area A, then the grand partition function is $\Xi = e^{\frac{pV+\phi A}{kT}}$, where ϕ is the spreading pressure. The difference in the number of molecules under the two conditions we define as the number of molecules adsorbed:

$$\bar{N}a = \bar{N} - \bar{N}_{o} \; . \tag{2.01}$$

An equation for $\bar{N}a$ is readily written down;

$$\bar{N}a = \left(\frac{\partial \ln \Xi^{*}}{\partial \ln \mathfrak{z}} \right)_{T,V} \; , \tag{2.02}$$

where $\Xi^{*} = \Xi / \Xi^{\circ}$, The activity of the gas $\mathfrak{z}$, is given by

$$\mathfrak{z} = e^{\mu/kT} / \lambda^{3} \tag{2.03}$$

where

$$\lambda = h/(2\pi mkT)^{1/2} \; , \tag{2.04}$$

m is the molecular mass and h is Planck's constant.

From Hill[28], one can write the two partition functions as

$$\Xi(T,V,A,\mathfrak{z}) = \sum_{N \geq 0} Z_{N} \mathfrak{z}^{N} / N! \; , \tag{2.05}$$

and

$$\Xi^{\circ}(T,V,z) = \sum_{N \geq 0} Z_N^{\circ} z^N / N! \quad , \tag{2.06}$$

where Z_N and Z_N° are the N particle configurational integrals which are given for a classical gas with pair interactions as

$$Z_N^{\circ} = \int\cdots\int_V \exp\left[-\beta \sum_{1 \leq i < j \leq N} \phi(r_{ij})\right] d\underline{r}^N \quad , \tag{2.07}$$

and

$$Z_N = \int\cdots\int_V \exp\left[-\beta\left(\sum_{i=1}^{N} \phi_s(\underline{r}_i) + \sum_{1 \leq i < j \leq N} \phi(r_{ij})\right)\right] d\underline{r}^N \quad . \tag{2.08}$$

One can expand the logarithms of (2.05) and (2.06) in a series for $(pV + \phi A)/kT$ and pV/kT respectively:

$$\ln \Xi = \frac{pV+\phi A}{kT} = V \sum_{j \geq 1} b_j z^j \quad , \tag{2.09}$$

where

$$\begin{aligned} 1!\, Vb_1 &= Z_1 \quad , \\ 2!\, Vb_2 &= Z_2 - Z_1^2 \quad , \\ 3!\, Vb_3 &= Z_3 - 3Z_1 Z_2 + 2Z_1^3 \quad , \\ &\text{etc.} \end{aligned} \tag{2.10}$$

and

$$\ln \Xi^{\circ} = \frac{pV}{kT} = V \sum_{j \geq 1} b_j^{\circ} z^j \quad , \tag{2.11}$$

where

$$1!\,Vb_1^{\circ} = Z_1^{\circ} = V$$
$$2!\,Vb_2^{\circ} = Z_2^{\circ} - Z_1^{\circ 2}$$
$$3!\,Vb_3^{\circ} = Z_3^{\circ} - 3Z_1^{\circ} Z_2^{\circ} + 2Z_1^{\circ 3} \qquad (2.12)$$

etc.

Performing the appropriate partial integrations on (2.02), one gets

$$\bar{N}a = \sum_{j\geq 1} Vj\,(b_j - b_j^{\circ})\,z^j. \qquad (2.13)$$

By expanding this equation in the activity to the second power and writing the b_j's and b_j°'s in terms of the Mayer f functions[3], one gets

$$\bar{N}a = z\int f_1 d\underset{\sim}{r}_1 + z^2 \iint (f_{12}f_2 + f_1 f_2 f_{12})\, d\underset{\sim}{r}_1 d\underset{\sim}{r}_2 + \ldots. \qquad (2.14)$$

Substituting (1.02) into (2.14), gives us the adsorption isotherm in terms of the activity and the irreducible cluster integrals[2,3]:

$$\bar{N}a = \beta_1 z + (\beta_2 + 2\beta_1\,\beta_1^{\circ})\,z^2 + \ldots, \qquad (2.15)$$
$$= B_{AS}\,z + C'_{AAS}\,z^2 + \ldots. \qquad (2.15a)$$

By inverting (2.11) to get the activity in a power series in the pressure, and then substituting the new series into (2.15), one can write the adsorption isotherm with the pressure as the independent variable rather than z:

$$\bar{N}a = \beta_1 \left(\frac{p}{kT}\right) + \left(\beta_2 + \tfrac{3}{2}\beta_1\,\beta_1^{\circ}\right) \left(\frac{p}{kT}\right)^2 + \ldots, \qquad (2.16)$$

$$= B_{AS} \left(\frac{p}{kT}\right) + C_{AAS} \left(\frac{p}{kT}\right)^2 + \ldots. \qquad (2.16a)$$

Equations (2.15) and (2.16) are both exact isotherms, but (2.16) is more useful as a working isotherm. At sufficiently high temperatures, all the f_{ij} vanish and only B_{AS} is important:

$$\bar{N}a = B_{AS} \left(\frac{p}{kT}\right) . \tag{2.17}$$

At lower temperatures, C_{AAS} assumes finite values and the isotherm is no longer linear in the pressure.

However, at these low temperatures the probability of finding an adsorbed molecule anywhere except in the immediate vicinity of a potential minimum becomes quite small. In this case, the three-dimensional integrals become unnecessarily cumbersome. It has been shown[29,30] that the configurational integrals can be split into two parts: three-dimensional integrals $Z_1^{(s)}$ representing single molecules on the surface; and a reduced configurational integral in the two dimensions parallel to the surface which give the contributions of lateral interactions to the properties of the adsorbed monolayer. We consider a uniform solid surface which is made up of N_s identical elements of area A_s which will be termed sites. Within each element, $\phi_s(\underline{r}_i)$ will vary with z_i, the perpendicular distance between the ith gas molecule and the surface of the solid, and will ordinarily vary with a two-dimensional vector, $\underline{r}_i$, lying in a plane parallel to the surface. If all N_s elements have identical $\phi_s(\underline{r}_i)$, then

$$Z_1^{(s)} = N_s Z_s , \tag{2.18}$$

where Z_s is the configurational integral for a single molecule over a site.

If one introduces a dimensionless quantity $\beta^{(2)}$ as

$$\mathcal{Z}^{(2)} = Z_1^{(s)} \mathcal{Z} \ , \tag{2.19}$$

then

$$\Xi^* = \sum_{N \geq 0} \frac{Z_N^{(s)}}{N! (Z_1^{(s)})^N} (\mathcal{Z}^{(2)})^N \ . \tag{2.20}$$

At temperatures near the boiling point of the adsorbate, the value of $-\phi_s(\underset{\sim}{r}_i)/kT$ are expected to be rather large ($\gtrsim 10$) at distances corresponding to the position of maximum attractive energy. The exponential of this function will be quite large in this region, so that one can make the approximation

$$Z_1^{(s)} = \iint_{Az_s} \exp\left[-\phi_s(\underset{\sim}{r}_i)/kT\right] d\underset{\sim}{r}_i \, dz_i \ , \tag{2.21}$$

where z_s is the distance over which ϕ_s is important. Also, since the probability of finding a gas atom at a distance z from the surface will have a very large maximum at or near $z=z_m$; where z_m is the position at which the maximum interaction energy is to be found, one is actually saying that the adsorbed film approximates a two-dimensional phase.

Steele[8] approximates $\phi_s(\underset{\sim}{r})$ in the region of its minimum by

$$\phi_s(\underset{\sim}{r}) = \varepsilon_{ls} + \frac{1}{2} k_z (z-z_m)^2 + \varepsilon_\tau(\underset{\sim}{\tau}) \tag{2.22}$$

where ε_{ls} is the potential minimum at the center of a site ($\underset{\sim}{\tau}=0$), $\varepsilon_\tau(\underset{\sim}{\tau})$ is the variation in ε_{ls} as an atom moves parallel to the surface, and the second term is a harmonic oscillator approximation for motion in the z direction. If ε_{ls} and the force constant, k_z, are large, the z integrations in the configurational integrals thus involve functions which have large maxima and are rapidly varying in the region of the maxima.

It is therefore appropriate to use the method of steepest descents to evaluate such integrals.

Steele has shown[8] that the ratio $Z_N^{(s)} / (Z_1^{(s)})^N$ can be written as

$$\frac{Z_N^{(s)}}{(Z_1^{(s)})^N} = \int\cdots\int_A P_o^{(N)} (\underset{\sim}{r}_1 \cdots \underset{\sim}{r}_N) \exp\left[-\sum_{1\le i<j\le N} \beta\phi_e(r_{ij})\right] \{ 1 + C(\underset{\sim}{r}_1 \cdots \underset{\sim}{r}_N) \}\, d\underset{\sim}{r}_1 \cdots d\underset{\sim}{r}_N \quad , \tag{2.23}$$

where $C(\underset{\sim}{r}_1 \cdots \underset{\sim}{r}_N)$ is a correction term for non-planarity, ie, $z \neq z_m$. $P_o^{(N)}$ is equal to the probability of finding N non-interacting molecules in elements of unit area at points $\underset{\sim}{r}_1 \cdots \underset{\sim}{r}_N$ on the surface, and is given by

$$P_o^{(N)} (\underset{\sim}{r}_1 \cdots \underset{\sim}{r}_N) = \frac{\exp\left[-\sum_{i=1}^{N} \varepsilon_\tau(\underset{\sim}{r}_i)/kT\right]}{\int\cdots\int_A \exp\left[-\sum_{i=1}^{N} \varepsilon_\tau(\underset{\sim}{r}_i)/kT\right] d\underset{\sim}{r}_1 \cdots d\underset{\sim}{r}_N} \quad . \tag{2.24}$$

If $\varepsilon_\tau(\underset{\sim}{r}_i)$, the potential barrier to motion across the surface, is zero, $P_o^{(N)} (\underset{\sim}{r}_1 \cdots \underset{\sim}{r}_N) = A^{-N}$. Neglecting the correction term for non-planarity, (2.23) becomes an equation for the 2N-dimensional configurational integral which corresponds to a generalized two-dimensional gas constrained to move in the plane defined by $z=z_m$.

The two-dimensional configurational integral is now given by

$$Z_N^{(2)} = \int\cdots\int_A P_o^{(N)} (\underset{\sim}{r}_1 \cdots \underset{\sim}{r}_N) \exp\left[-\sum_{i\le i<j\le N} \phi_e (r_{ij})/kT\right], \tag{2.25}$$

and the grand partition function becomes

$$\Xi^* = \sum_{N \ge 0} \frac{Z_N^{(2)} (\mathcal{Z}^{(2)})^N}{N!} \tag{2.26}$$

The adsorption isotherm is obtained from

$$\bar{N}a = \left(\frac{\partial \ln \Xi^*}{\partial \ln z^{(2)}}\right)_{T,V} ; \qquad (2.27)$$

and it is now evident that the quantity denoted by $z^{(2)}$ does play the role of an activity for a two-dimensional system. The logarithm of Ξ^* is given by

$$\ln \Xi^* = Z_1^{(2)} z^{(2)} + (Z_2^{(2)} - (Z_1^{(2)})^{(2)}) \frac{(z^{(2)})}{2} + \ldots, \qquad (2.28)$$

with $Z_1^{(2)} = 1$. Performing the partial integrations indicated by (2.30), the adsorption isotherm becomes

$$\bar{N}a = \beta_1^{(2)} z^{(2)} + \beta_2^{(2)} (z^{(2)})^2 + \beta_3^{(2)} (z^{(2)})^3 + \ldots, \qquad (2.29)$$

where

$$\beta_1^{(2)} = 1, \qquad (2.30)$$

$$\beta_2^{(2)} = \int_A \ldots \int P_o^{(2)} (\underset{\sim}{r}_1, \underset{\sim}{r}_2) f_{12} \, d\underset{\sim}{r}_1 \, d\underset{\sim}{r}_2 , \qquad (2.31)$$

$$\beta_3^{(2)} = \iiint_A P_o^{(3)} (\underset{\sim}{r}_1, \underset{\sim}{r}_2, \underset{\sim}{r}_3) (f_{12} f_{13} f_{23} + 3 f_{12} f_{13}) \, d\underset{\sim}{r}_1 d\underset{\sim}{r}_2 d\underset{\sim}{r}_3, \qquad (2.32)$$

and f_{ij} are now defined in two dimensions as

$$f_{ij} = \exp [- \beta \phi_e (r_{ij})] - 1, \qquad (2.33)$$

Equation (2.29) can be inverted to give $z^{(2)}$ as a power series in $\bar{N}a$:

$$z^{(2)} = \bar{N}a - \beta_2^{(2)} \bar{N}a^2 + (2(\beta_2^{(2)})^2 - \beta_3^{(2)}) \bar{N}a^3 - \ldots . \qquad (2.34)$$

From equations (2.09) and (2.11), one has for the spreading pressure

$$\frac{\phi A}{kT} = \ln \Xi^{*} . \qquad (2,35)$$

Then by substituting (2,28) into (2,35), one gets an expression for the spreading pressure. This can be converted to a two-dimensional equation of state by eliminating $z^{(2)}$ with equation (2,34). The result is

$$\frac{\phi A}{\bar{N}akT} = 1 - \frac{\beta_2^{(2)}}{2}\left(\frac{\bar{N}a}{A}\right) + \frac{(3\beta_2^{(2)} - 2\beta_3^{(2)})}{3}\left(\frac{\bar{N}a}{A}\right)^2 + \ldots, \qquad (2,36)$$

or

$$\frac{\phi A}{\bar{N}akT} = 1 + B^{(2)}\left(\frac{\bar{N}a}{A}\right) + C^{(2)}\left(\frac{\bar{N}a}{A}\right)^2 + \ldots, \qquad (2,37)$$

where

$$\frac{B^{(2)}}{A} = -\frac{\beta_2^{(2)}}{2} , \qquad (2,38)$$

$$\frac{C^{(2)}}{A^2} = (\beta_2^{(2)})^2 - \frac{2}{3}\beta_3^{(2)} . \qquad (2,39)$$

The two-dimensional virial coefficients are closely analogous to the three-dimensional coefficients and, just as in the three-dimensional case, are the "irreducible cluster integrals" first introduced by Mayer[3]. One can thus rewrite (2,29) as

$$\bar{N}a = z^{(2)} - (2B^{(2)}/A)(z^{(2)})^2 + 3(2(B^{(2)})^2/A^2 - \frac{1}{2}C^{(2)}/A^2)(z^{(2)})^3 + \ldots . \qquad (2,40)$$

If we compare this with the exact high temperature isotherm equation, (2.15), it is readily seen that

$$B_{AS} \longrightarrow \int_A \int \bar{z}_s \exp\left[-\beta\phi_s(\underset{\sim}{r})\right] d\underset{\sim}{r}dz = Z_1^{(\bar{s})}, \tag{2.41}$$

$$C'_{AAS} \longrightarrow -(2B^{(2)}/A)\,(Z_1^{(s)})^2. \tag{2.42}$$

These equations can be rearranged to give

$$-C'_{AAS}/2B_{AS}^2 \longrightarrow B^{(2)}/A. \tag{2.43}$$

CHAPTER 3

QUANTUM STATISTICAL EQUATION OF STATE [21,23,25,31,32]

For a closed system in equilibrium at temperature T, one can write the classical probability density $P_N(\underset{\sim}{r}^N, \underset{\sim}{p}^N)$ of the canonical ensemble as

$$P_N(\underset{\sim}{r}^N, \underset{\sim}{p}^N) = \frac{1}{N! h^{3N} Q_N} \exp(-H_N / kT), \tag{3.01}$$

where H is the Hamiltonian for an N particle system and Q_N a normalizing constant, the canonical partition function. It can be determined by the normalizing condition

$$\iint P_N \, d\underset{\sim}{r}^N \, d\underset{\sim}{p}^N = 1, \tag{3.02}$$

or

$$Q_N = \frac{1}{N! h^{3N}} \iint \exp(-H_N/kT) \, d\underset{\sim}{r}^N \, d\underset{\sim}{p}^N. \tag{3.03}$$

Classically, one writes the Hamiltonian as a sum of the kinetic energy $\sum_i p_i^2 / 2m$, and a potential energy $\phi(\underset{\sim}{r}^N)$ which depends on the configuration of all the molecules of the system. Carrying out the integrations over the momenta yields the configurational distribution function

$$P_N(\underset{\sim}{r}^N) = \frac{1}{Z_N} \exp(-\phi(\underset{\sim}{r}^N)/kT), \tag{3.04}$$

where Z_N is the configurational partition function,

$$Z_N = N! \, \lambda^{3N} \, Q_N. \tag{3.05}$$

Defining a function $W_N(\underset{\sim}{r}^N)$ by

$$W_N = \lambda^{-3N} \exp(-\phi(\underset{\sim}{r}^N)/kT), \tag{3.06}$$

the configurational distribution function becomes

$$P_N(\underset{\sim}{r}^N) = \frac{1}{N!Q_N} W_N(\underset{\sim}{r}^N), \tag{3.07}$$

and from the normalising condition we have:

$$Q_N = \frac{1}{N!} \int W_N d\underset{\sim}{r}^N. \tag{3.08}$$

Thus far the development has been restricted to classical systems. However there are two types of quantum effects which have to be considered under certain conditions: (i) diffraction effects, which result from the wave nature of the molecules and are important when the de Broglie wave length associated with the molecules is of the order of magnitude of the molecular diameter; (ii) symmetry effects, which result from the statistics of the particles and are of importance when the de Broglie wave length of the molecule is of the order of magnitude of the average distance between the molecules in the gas. At room temperature the diffraction effects are measurable in helium and hydrogen but unimportant for heavier gases. At lower temperatures the quantum deviations associated with these effects are quite appreciable for helium and hydrogen and of some importance for the heavier gases. Symmetry effects are important only at high densities or very low temperatures. Deviations from classical behavior depend upon the magnitude of the quantity $\Lambda^* = h/\sigma (m\varepsilon)^{1/2}$. This quantity is the ratio of the de Broglie wavelength (corresponding to a system of reduced mass μ and energy ε) to the collision diameter σ, and is characteristic for each substance.

Quantally the role of the classical probability density is taken over by the probability density matrix,

$$\mathcal{P}_N (\underset{\sim}{r}^N, \underset{\sim}{r}^{N'}) = \quad \langle \psi^* (\underset{\sim}{r}^{N'} , t) \ \psi(\underset{\sim}{r}^N, t) \rangle \ . \qquad (3.09)$$

The density matrix is independent of the particular system of wave functions chosen, since it is the average value $\langle \psi^* (\underset{\sim}{r}^{N'}) \ \psi(\underset{\sim}{r}^N) \rangle$ over all systems of the ensemble. This property of invariance of the density matrix is a very useful one in that it allows $\mathcal{P}_N(\underset{\sim}{r}^N, \underset{\sim}{r}^{N'})$ to be written in terms of any orthonormal set of basis functions spanning the whole space. The probability density matrix is a function of the two sets of N position vectors $\underset{\sim}{r}^N$ and $\underset{\sim}{r}^{N'}$. The classical integration over momenta, leading to the configurational probability density $P_N(\underset{\sim}{r}^N)$, is replaced in the quantum case by the taking of the diagonal element $\mathcal{P}_N(\underset{\sim}{r}^N, \underset{\sim}{r}^N)$. We assume the density matrix to be normalised, so that

$$\int \mathcal{P}_N (\underset{\sim}{r}^N, \underset{\sim}{r}^N) \, d\underset{\sim}{r}^N = 1. \qquad (3.10)$$

If we define a probability operator $\mathcal{P}$ such that the probability density matrix elements can be written as

$$\mathcal{P}_N (\underset{\sim}{r}^N, \underset{\sim}{r}^{N'}) = \sum_\nu \ \phi_\nu^* \ (\underset{\sim}{r}^{N'} \ ) \ \mathcal{P}_{\phi_\nu} (\underset{\sim}{r}^N), \qquad (3.11)$$

then it can be shown by means of the quantum Liouville equation[23] that $\mathcal{P}$ must be a function only of the Hamiltonian operator $\mathcal{H}_N(\underset{\sim}{r}^N, \underset{\sim}{p}^N)$:

$$\mathcal{P} = \frac{1}{Q_N} \quad \exp \ (- \mathcal{H}_N / kT) \ , \qquad (3.12)$$

where $\mathcal{P}_j = -i\hbar\, \partial/\partial r_j$ is the momentum operator, and the operator $\exp(-\mathcal{H}/kT)$ is defined as $\sum -(\mathcal{H}/kT)^n/n$. From (3.11) and (3.12), the density matrix is

$$\rho_N(r^N, r^{N'}) = \frac{1}{Q_N} \sum_\nu \phi_\nu^*(r^{N'}) \exp(-\mathcal{H}_N/kT)\ \phi_\nu(r^N), \qquad (3.13)$$

and the diagonal elements are

$$\rho_N(r^N, r^N) = \frac{1}{Q_N} \sum_\nu \phi_\nu^*(r^N) \exp(-\mathcal{H}_N/kT)\ \phi_\nu(r^N). \qquad (3.14)$$

This expression is the quantum analogue of the classical configurational distribution function. (3.14) can be put into a form analogous to (3.07) by defining

$$\int \mathcal{W}_N(r^N)\, dr^N = N!\ \mathrm{Tr}\ \exp(-\mathcal{H}_N/kT), \qquad (3.15)$$

whence

$$\rho_N(r^N, r^N) = \frac{1}{N! Q_N}\ \mathcal{W}_N(r^N). \qquad (3.16)$$

From (3.10),

$$Q_N = \int \left(\sum_\nu \phi_\nu^*(r^N) \exp(-\mathcal{H}_N/kT)\ \phi_\nu(r^N) \right) dr^N$$
$$= \frac{1}{N!} \int \mathcal{W}_N(r^N)\, dr^N, \qquad (3.17)$$

corresponding to (3.07).

The Slater sum[33,34] $\mathcal{W}_N(r^N)$ is the exact quantum mechanical analogue of the Boltzmann Factor $W_N(r^N)$, and at high temperatures, where quantum deviations are small, $\mathcal{W}_N \longrightarrow W_N$. This can be proven by using the invariance property of ρ_N for the system of orthonormal eigenfunctions used. Since the $\phi_\nu(r^N)$ form a complete orthonormal set,

$$\sum_{\nu} \phi_{\nu}^{*}(\underset{\sim}{r}'_{\ell}) \, \phi_{\nu}(\underset{\sim}{r}_{\ell}) = \prod_{1 \le \ell}^{N} \delta(\underset{\sim}{r}'_{\ell} - \underset{\sim}{r}_{\ell}), \tag{3.18}$$

where $\delta(\underset{\sim}{r}'_{\ell} - \underset{\sim}{r}_{\ell})$ is the Dirac volume δ function. The Slater sum can therefore be written as

$$\mathcal{W}_N(\underset{\sim}{r}^N) = \left[\exp(-\mathcal{H}_N/kT) \sum_P (\pm 1)^P \prod_{\ell} \delta(\underset{\sim}{r}'_{\ell} - \underset{\sim}{r}_{p\ell})\right]_{\underset{\sim}{r}'_{\ell} = \underset{\sim}{r}_{\ell}}, \tag{3.19}$$

where $\mathcal{H}_N$ operates only on the $\underset{\sim}{r}_{\ell}$, and after this operation all $\underset{\sim}{r}'_{\ell}$ are set equal to the corresponding $\underset{\sim}{r}_{\ell}$. The $\phi_{\nu}(r^N)$ have been properly symmetrized by summing over all permutations P of the indices. $\underset{\sim}{r}_{p\ell}$ indicates the 3N-dimensional vector resulting from the application of this permutation to the vector $\underset{\sim}{r}_{\ell}$. The +1 is for the symmetrical case (Bose-Einstein statistics) and -1 for the antisymmetrical case (Fermi-Dirac statistics).

We shall consider first the ideal gas, for which the Hamiltonian is just the kinetic energy operator,

$$\mathcal{H}_N = \mathcal{T}_N = -(\hbar^2/2m) \sum_j \nabla_j^2, \tag{3.20}$$

where ∇_j^2 is the Laplacian of the jth particle. Writing the δ function in terms of its Fourier integral, one gets

$$\exp(-\mathcal{T}/kT)\, \delta(\underset{\sim}{r}' - \underset{\sim}{r}) = \iiint_{-\infty}^{+\infty} \exp[-(\lambda^2 k^2/4\pi) + 2\pi i \underset{\sim}{k}\cdot(\underset{\sim}{r}' - \underset{\sim}{r})] d\underset{\sim}{k}$$

$$= \lambda^{-3} \exp[-\pi(\underset{\sim}{r}' - \underset{\sim}{r})^2 / \lambda^2], \tag{3.21}$$

and from (3.19),

$$\mathcal{W}_N^{\circ}(\underset{\sim}{r}^N) = \lambda^{-3N} \sum_P (\pm 1)^P \exp\left[-\frac{\pi}{\lambda^2} \sum_{\ell} (\underset{\sim}{r}_{\ell} - \underset{\sim}{r}_{p\ell})^2\right]. \tag{3.22}$$

Throughout we shall adopt the convention that the upper sign refers to

Bose-Einstein statistics.

Since the identity permutation operator causes the argument of the exponent to vanish, $\mathcal{W}_N^\circ = \lambda^{-3N}$ if the symmetry of the eigenfunctions has no influence. This value λ^{-3N} is the value of W_N for an ideal gas ($\phi(r^N) = 0$).

The distance over which the molecules influence each other due to the symmetry of the wave functions is of the order of magnitude $\lambda = h/(2mkT)^{1/2}$ which, except for a numerical factor, is the de Broglie wavelength of the molecular motion at a temperature T. As this wavelength become much smaller than the molecular diameter at high temperatures, these deviations due to statistical effects become very small. Thus for an ideal gas at high temperatures $\mathcal{W}_N^\circ(\underset{\sim}{r}^N) \longrightarrow W_N^\circ(\underset{\sim}{r}^N)$.

For a real gas, the complete Hamiltonian must be substituted into (3.19). The proof that the Slater sum now approaches the Boltzmann factor at high temperatures has been given by Kirkwood, who obtained a series expansion for $\mathcal{W}_N$;

$$\mathcal{W}_N(\underset{\sim}{r}^N) = W_N(\underset{\sim}{r}^N)\{1+\lambda^2\sum_j w_2^{(j)} + \lambda^4 \sum_j w_4^{(j)} + \cdots\} + \mathcal{W}_N^\circ(\underset{\sim}{r}^N) \tag{3.23}$$

in which

$$w_2^{(j)} = \frac{-\beta}{24\pi}\left[\nabla_j^2\phi - \frac{\beta}{2}(\underset{\sim}{\nabla}_j\phi)^2\right] \tag{3.24}$$

$$w_4^{(j)} = \frac{1}{960\pi^2}\beta\left\{\nabla_j^4\phi - \frac{\beta}{6}\left[2\nabla_j^2(\underset{\sim}{\nabla}_j\phi)^2 + 8\,\underset{\sim}{\nabla}_j\phi\cdot\underset{\sim}{\nabla}_j^3\phi\right.\right.$$

$$+5\,(\nabla_j^2\phi)^2] + \frac{\beta}{6}^2\,[5\nabla_j^2\phi\,(\underset{\sim}{\nabla}_j\phi)^2 + 3\,\underset{\sim}{\nabla}_j\phi\cdot\underset{\sim}{\nabla}_j\,(\underset{\sim}{\nabla}_j\phi)^2]$$

$$-\frac{5}{24}\,\beta^3\,(\underset{\sim}{\nabla}_j\phi)^4\,\}\quad . \tag{3.25}$$

The series (3.23) converges when the factor $h^2/m\,kT$, which is of the order of the square of the thermal de Broglie wavelength, is small. Thus (3.23) offers a good approximation to $\mathcal{W}_N(\underset{\sim}{r}^N)$ when the temperature is high and the quantum deviations small.

We now consider the evaluation of the two-dimensional second virial coefficient, $B^{(2)}$. This case is completely analogous to the three-dimensional one[23] if the following changes are made:

1. $\underset{\sim}{r}$ becomes the two-dimensional vector $\underset{\sim}{\tau}$, where $\underset{\sim}{\tau}$ is a cylindrical coordinate. Hence, the Laplacian of the ith particle becomes

$$\nabla_i^2 = \tau^{-1}\,(\partial/\partial\underset{\sim}{\tau})\,\tau\,(\partial/\partial\underset{\sim}{\tau}). \tag{3.26}$$

2. The three-dimensional volume is replaced by the area element $2\pi\tau\,d\tau$.

The two dimensional virial coefficient can then be written as

$$B^{(2)} = -\frac{N\lambda^4}{2A}\iint\,[\mathcal{W}_2(\underset{\sim}{\tau}_1,\underset{\sim}{\tau}_2) - \mathcal{W}_1(\underset{\sim}{\tau}_1)\mathcal{W}_1(\underset{\sim}{\tau}_2)]$$

$$d\underset{\sim}{\tau}_1\,d\underset{\sim}{\tau}_2 \tag{3.27}$$

For a perfect two-dimensional gas one obtains immediately

$$\mathcal{W}_N^{\circ}(\underset{\sim}{\tau}^N) = \lambda^{-2N}\sum_P(\pm)^P\exp\left[-\frac{\pi}{\lambda^2}\sum_i(\underset{\sim}{\tau}_i - \underset{\sim}{\tau}_{P_i})\right] \tag{3.28}$$

For a real gas one must employ the complete Hamiltonian to obtain the

two-dimensional analogues of (3.23) - (3.25). Writing the Slater sum for two particles and substituting into (3.27), one finds for the second virial coefficient,

$$B^{(2)} = (B_{cl}^{(2)} + B_{I}^{(2)} + B_{II}^{(2)} + \dots) \mp B_{perf}^{(2)} \qquad (3.29)$$

where $B_{cl}^{(2)}$ is the classical contribution, $B_{I}^{(2)}$ and $B_{II}^{(2)}$ the first and second quantum corrections proportional to λ^2 and λ^4 respectively, and $B_{perf}^{(2)}$ the quantum perfect gas term arising from $\mathcal{Q}_N^\circ$.

We want to evaluate $B^{(2)}$ using a completely general power-law potential function, which can be written as[35]

$$\phi(\tau^*) = -\gamma\varepsilon\,[A\tau^{*-a} + B\tau^{*-b} + C\tau^{*-c} + \dots - Z\tau^{*-z}] \,. \qquad (3.30)$$

The perfect gas term, which is independent of the potential, is done first. Using (3.27) and (3.28), and integrating, one gets,

$$B_{perf}^{(2)} = \mp \frac{N}{2A} \iint \exp\left[-\frac{2}{\lambda^2}(\underset{\sim}{r}_1 - \underset{\sim}{r}_2)^2\right] d\underset{\sim}{r}_1 d\underset{\sim}{r}_2 \,,$$

$$= \mp \frac{N\lambda^2}{4} \,,$$

$$= \mp \frac{N\beta h^2}{8\pi m} \,. \qquad (3.31)$$

The remaining terms are found by substituting the two-dimensional analogues of (3.23) - (3.25) into (3.27):

$$B_{cl}^{(2)} = -\pi N \int_0^\infty [\exp(-\beta\phi) - 1]\, \tau d\tau \,, \qquad (3.32)$$

$$B_I^{(2)} = \frac{\pi N \hbar^2}{12\mu} \int_0^\infty \exp(-\beta\phi)\left[\nabla^2\phi - \frac{\beta}{2}(\nabla\phi)^2\right]\tau d\tau , \qquad (3.33)$$

$$B_{II}^{(2)} = -\frac{\pi N \hbar^4 \beta^3}{240\,\mu^2} \int_0^\infty \exp(-\beta\phi)\{\nabla^4\phi - \frac{\beta^2}{6}[2\nabla^2(\nabla\phi)^2 + 8\nabla\phi\cdot\nabla^3\phi + 5(\nabla^2\phi)^2] + \frac{\beta^2}{6}[5\nabla^2\phi(\nabla\phi)^2 + 3\nabla\phi\cdot\nabla(\nabla\phi)^2] - \frac{5}{24}\beta^3(\nabla\phi)^4\}\tau d\tau , \qquad (3.34)$$

where μ is the reduced mass.

It is desirable to write the second virial coefficient in reduced form:

$$B^{(2)*} = [B_{cl}^{(2)*} + \Lambda^{*2} B_I^{(2)*} + \Lambda^{*4} B_{II}^{(2)*} + \ldots] \mp \Lambda^{*2} B_{perf}^{(2)*} , \qquad (3.35)$$

where

$$B^{(2)} = \frac{1}{2}\pi N \sigma^2 B^{(2)*} ; \quad \Lambda^* = h/\sigma(m\varepsilon)^{1/2} . \qquad (3.36)$$

Then if we introduce a reduced temperature, defined by $T^* = (\beta\varepsilon)^{-1}$, equation (3.31) becomes

$$B_{perf}^{(2)*} = (4\pi^{1/2} T^*)^{-1} , \qquad (3.37)$$

and after a series of partial integrations, equations (3.32) - (3.34) become

$$B_{cl}^{(2)*} = -\beta\sigma^{-2} \int_0^\infty \exp(-\beta\phi)\,\phi'\,\tau^2\,d\tau , \qquad (3.38)$$

$$B_I^{(2)*} = \beta(24\pi^2 T^*)^{-1} \int_0^\infty \exp(-\beta\phi)\nabla^2\phi\,\tau d\tau , \qquad (3.39)$$

$$B_{11}^{(2)*} = -(\beta\sigma^2/20)(24\pi^2T^*)^{-2}\int_0^\infty \exp(-\beta\phi)\{-5\phi'''' + \frac{12}{\tau^2}\phi'' - \frac{12}{\tau^3}\phi' + 7\beta(\phi'')^2\}\,\tau d\tau\,. \tag{3.40}$$

When equation (3.30) for the potential is introduced, (3.38) - (3.40) can be integrated analytically to give

$$B_{cl}^{(2)*} = -\sum_{j,k,l,\ldots\geq 0}\frac{2}{z}\frac{A^jB^kC^l\ldots}{j!k!l!\ldots}\,Z^{\frac{-(aj+bk+cl+\ldots-2)}{z}}\left(\frac{\gamma}{T}\right)^{\frac{(z-a)j+(z-b)k+(z-c)l+\ldots+2}{z}}\Gamma\left(\frac{aj+bk+cl+\ldots-2}{z}\right) \tag{3.41}$$

$$B_1^{(2)*} = (24\pi^2T^*)^{-1}\left[z + \sum_{j,k,l,\ldots\geq 0}{}'(\lambda^{(2)}/z)\frac{A^jB^kC^l\ldots}{j!k!l!\ldots}Z^{\frac{-(aj+bk+cl+\ldots)}{z}}\left(\frac{\gamma}{T^*}\right)^{\frac{(z-a)j+(z-b)k+(z-c)l+\ldots}{z}}\Gamma\left(\frac{aj+bc+cl+\ldots}{z}\right)\right], \tag{3.42}$$

where

$$\lambda^{(2)} = \sum_n nS_n(z-n), \qquad n=a,b,c,\ldots.$$

$$S_n = j,k,l,\ldots, \tag{3.43}$$

$$B_{11}^{(2)*} = -\frac{(24\pi^2 T^*)^{-2}}{20z} \sum_{j,k,l,\ldots \geq 0}{}' (\mu^{(2)} + \nu^{(2)} + \rho^{(2)} + \xi^{(2)})$$

$$\frac{A^j B^k C^l \ldots}{j!\,k!\,l!\ldots} \; z^{\frac{-(aj+bk+cl+\ldots+2)}{z}} \; \left(\frac{\gamma}{T^*}\right)^{\frac{(z-a)j+(z-b)k+(z-c)l+\ldots-2}{z}}$$

$$\Gamma\left(\frac{aj+bk+cl+\ldots+2}{z}\right), \tag{3.44}$$

where

$$\mu^{(2)} = 7 \sum_m [mS_m (z-m)]^2$$

$$\nu^{(2)} = \sum_m mS_m \{7(z+1)^2 (z+4) - 7(m+1)[m(m+1)+4(z+1)] + 12(z-m) - 5[(z+1)(z+2)(z+3)-(m+1)(m+2)(m+3)]\} \tag{3.46}$$

$$\rho^{(2)} = 14 \sum_{r \neq n} nr \; S_n S_r \; [(z+1)(z-n-r-1) + (n+1)(r+1)] \tag{3.47}$$

$$\xi^{(2)} = (z+1)(z+2)[14(z+1) - 10(z+3)] + 24(z+2) \tag{3.48}$$

The prime on the summation indicates that the term j=o, k=o, etc, is omitted, which is necessitated by the fact that $\Gamma(0)$ is not defined. This leading zeroth term is a constant, and just gives the z appearing before the summation.

The various contribution to $B^{(2)*}$ have been computed at values of reduced temperature in the region $0.3 \leq T^* \leq 100$, using the two effective potentials (1.14) and (1.16) and numerical tables are given in Appendix 1. For (1.14) several different values of n in the range $0 \leq |n| \leq 0.05$ have been used. It is easy to show that by renormalizing the parameters in (1.16), this equation can be written in the usual (12,6) form,

$$\phi(\tau_{12}) = 4\,\varepsilon_2\,(\tau_2^{*-12} - \tau_2^{*-6}), \tag{3.49}$$

with
$$\varepsilon_2 = \xi^2\,\varepsilon\,,\quad \sigma_2 = \xi^{-1/6}\,\sigma\,,$$
$$\tau_2^{*} = \tau_{12}/\sigma_2. \tag{3.50}$$

Therefore in using this Appendix, it is to be understood that effective parameters must be employed for this potential.

We now wish to consider the evaluation of the second gas-surface virial coefficient. The total quantum B_{AS}, taken to order $\hbar^4$ in the Wigner-Kirkwood expansion, is given by

$$B_{AS} = B_{AS}^{cl} + B_{AS}^{I} + B_{AS}^{II} \pm B_{AS}^{perf}\,, \tag{3.51}$$

or in reduced form,

$$B_{AS}^{*} = (B_{AS}^{cl\,*} + \Lambda^{*2}\,B_{AS}^{I\,*} + \Lambda^{*4}\,B_{AS}^{II\,*} \pm \Lambda^{*}\,B_{AS}^{perf\,*}) \tag{3.52}$$

where $B_{AS} = Az_o\,B_{AS}^{*}$. Substituting the correct Slater sum, one gets for the various contributions to B_{AS}:

$$B_{AS}^{cl} = \int_{V_{geo}} [\exp(-\beta\phi_s) - 1]\,dV, \tag{3.53}$$

$$B_{AS}^{I} = \frac{\hbar^2\beta^2}{12m} \int_{V_{geo}} \exp(-\beta\phi_s)\,[\nabla^2\phi_s - (\tfrac{\beta}{2})\,(\underset{\sim}{\nabla}\phi_s)^2]\,dV, \tag{3.54}$$

$$B_{AS}^{II} = \frac{\hbar^4\beta^3}{240\,m^3} \int_{V_{geo}} \exp(-\beta\phi_s)\{\nabla^4\phi_s - \frac{\beta}{6}[2\nabla^2(\underset{\sim}{\nabla}\phi_s)^2$$

$$+8\,\underset{\sim}{\nabla}\phi_s \cdot \underset{\sim}{\nabla}^3\phi_s + 5\,(\nabla^2\phi_s)^2] + \frac{\beta^2}{6}\,[5\nabla^2\phi_s\,(\underset{\sim}{\nabla}\phi_s)^2 + 3\underset{\sim}{\nabla}\phi_s \cdot \underset{\sim}{\nabla}(\underset{\sim}{\nabla}\phi_s)^2] - \frac{5\beta^3}{24}\,(\underset{\sim}{\nabla}\phi_s)^4\,\}dV; \tag{3.55}$$

where $\beta = 1/kT$ and m is the molecular mass. ϕ_s is the interaction potential between an isolated gas molecule and the solid in the differential volume element dV, and we shall use the following approximation for this quantity. If one assumes that the gas molecules interact with individual atoms of the solid through a general Lennard-Jones potential, then

$$\phi(r) = [n/(m-n)]\,(n/m)^{m/(n-m)}\,\varepsilon_{ij}\,[(\sigma/r)^m - (\sigma/r)^n]. \tag{3.56}$$

We now assume the solid to be semi-infinite (i.e., infinite in x and y, and bounded by the plane z=o) and to obey the continuum model (i.e., uniform distribution of matter). Equation (3.51) can then be integrated over the three-dimensions of the solid to yield,

$$\phi_s(z) = (\beta/(\beta-\alpha))\,(\beta/\alpha)^{\alpha/(\beta-\alpha)}\,\varepsilon_{ls}[(z_o/z)^\alpha - (z_o/z)^\beta]. \tag{3.57}$$

Now, ε_{ls} is the maximum energy of gas-surface interaction, z_o is the distance between a gas atom and the plane surface at zero net interaction energy, and α and β are equal to n-3 and m-3, respectively. Substituting (3.52) into (3.48) - (3.50), and performing the analytic integrations, gives

$$B_{AS}^{cl\,*} = Az_o \sum_{j\geq o} (\beta j!)^{-1}\,(\gamma/T^*)^{\frac{j(\beta-\alpha)+1}{\beta}}\,\Gamma\left(\frac{j\alpha-1}{\beta}\right), \tag{3.58}$$

$$B_{AS}^{1\,*} = -Az_o\,\frac{1}{4}\,(24\pi^2T^*)^{-1} \sum_{j\geq o} \frac{(ja+b)}{\beta j!}\,(\gamma/T^*)^{\frac{j(\beta-\alpha)-1}{\beta}}\,\Gamma\left(\frac{j\alpha+1}{\beta}\right), \tag{3.59}$$

Where $a' = \alpha(\beta-\alpha)$ and $b' = \beta+1$,

$$B_{AS}^{II\,*} = Az_o \frac{1}{160} (24\pi^2 T^*)^{-2} \sum_{j\geq o} \frac{(j^2 a + jb + c)}{\beta j!} \left(\frac{\gamma}{T^*}\right)^{\frac{j(\beta-\alpha)-3}{\beta}} \Gamma\left(\frac{j\alpha+3}{\beta}\right), \tag{3.60}$$

where $a = -7\alpha^2 (\alpha-\beta)^2$ (3.61)

$$b = 5\alpha \{(\beta+1)(\beta+2)(\beta+3) - (\alpha+1)(\alpha+2)(\alpha+3)\} - 7(\beta+1)\alpha [(\beta+1)(\beta+6) - (\alpha+1)6] + 7\alpha^2 (\alpha+1)^2, \tag{3.62}$$

$$c = 3(\beta+1)(\beta+3)[3-2\beta], \tag{3.63}$$

and $\gamma = (\beta/(\beta-\alpha))(\beta/\alpha)^{\alpha/(\beta-\alpha)}$. (3.64)

Three different models for the interaction potential will be examined to analyse the data available for gas-solid interactions. The first of these is an inverse ninth-power repulsion, inverse cube attraction law (9,3) which results from a three-fold integration of a Lennard-Jones (12,6) potential. The layer structure of graphite suggests that maybe a better model for this solid could be obtained by integrating over the atoms of the surface plane only. The large distance between basal planes, compared to the relatively short in-plane distance between carbon atoms makes the contribution from the first layer of atoms of much the greatest importance at distances close to the surface, while contributions to the interaction energy from the underlying planes become relatively important only when the total interaction energy becomes small anyway. Such an integration of a (12,6) potential over an infinite plane leads to a (10,4) potential. Finally, since the repulsive forces are really caused by orbital overlap, and are thus short ranged, when an adsorbed atom is directly over a surface atom there is only a repulsion due to the single-

pair interaction. Thus the third model used is a (12,3) potential, corresponding to a three-fold integration of the attractive part of the potential only.

$B_{AS}^{cl\,*}$ and $B_{AS}^{l\,*}$ values have been published previously[20] and a table of $B_{AS}^{ll\,*}$ values, computed over a T^* range of $.1 \leq T^* \leq 1.0$, is given in Appendix II.

CHAPTER 4

THEORETICAL COMPARISON OF THE (12,6) AND (12,6,3) MODELS FOR $B^{(2)*}$.

From the tables in Appendix I, one can construct curves of the reduced two-dimensional second virial coefficient $B^{(2)*}$ as a function of reduced temperature T^*, once values for the quantum parameter Λ^* and the perturbational parameter η have been chosen. For the purpose of comparing the (12,6) and (12,6,3)potential energy models it is convenient to choose a system which displays fairly large quantum deviations. The three Bose-Einstein gases which display the largest quantum effects are He, H_2, and D_2. Therefore we consider a hypothetical Bose-Einstein gas (HBEG) with a Λ^* value of 1.8, which is the average value of Λ^* for the three gases mentioned above. Accordingly, Figure 1 presents classical and Bose-Einstein quantum curves of log $(1+|B^{(2)*}|)$ versus T^* for HBEG, as predicted by the two potential models. However, it is not appropriate to use the same value for the (12,6) model since the potential parameters have been renormalized. Theoretical estimates[24] for ε_2 predict that $\varepsilon_2 \simeq 0.9\varepsilon$ which results in an effective Λ^*_2 value of 1.9. To choose an appropriate η value we have noted that although theoretical predictions of the magnitude of this quantity for the rare gases fall in the range $0.04 \leq |\eta| \leq .07$, empirically determined values are always somewhat less[12], and we have therefore arbitrarily chosen $\eta = -0.05$. We feel this to be a reasonable upper bound for this parameter.

As shown in Figure 1, the quantum curves for both models converge to the classical limit at high temperatures as expected. The quantum

FIGURE 1

Reduced two-dimensional second virial coefficient for a hypothetical Bose-Einstein gas as a function of reduced temperature. Comparison of (12,6) and (12,6,3) potential models.

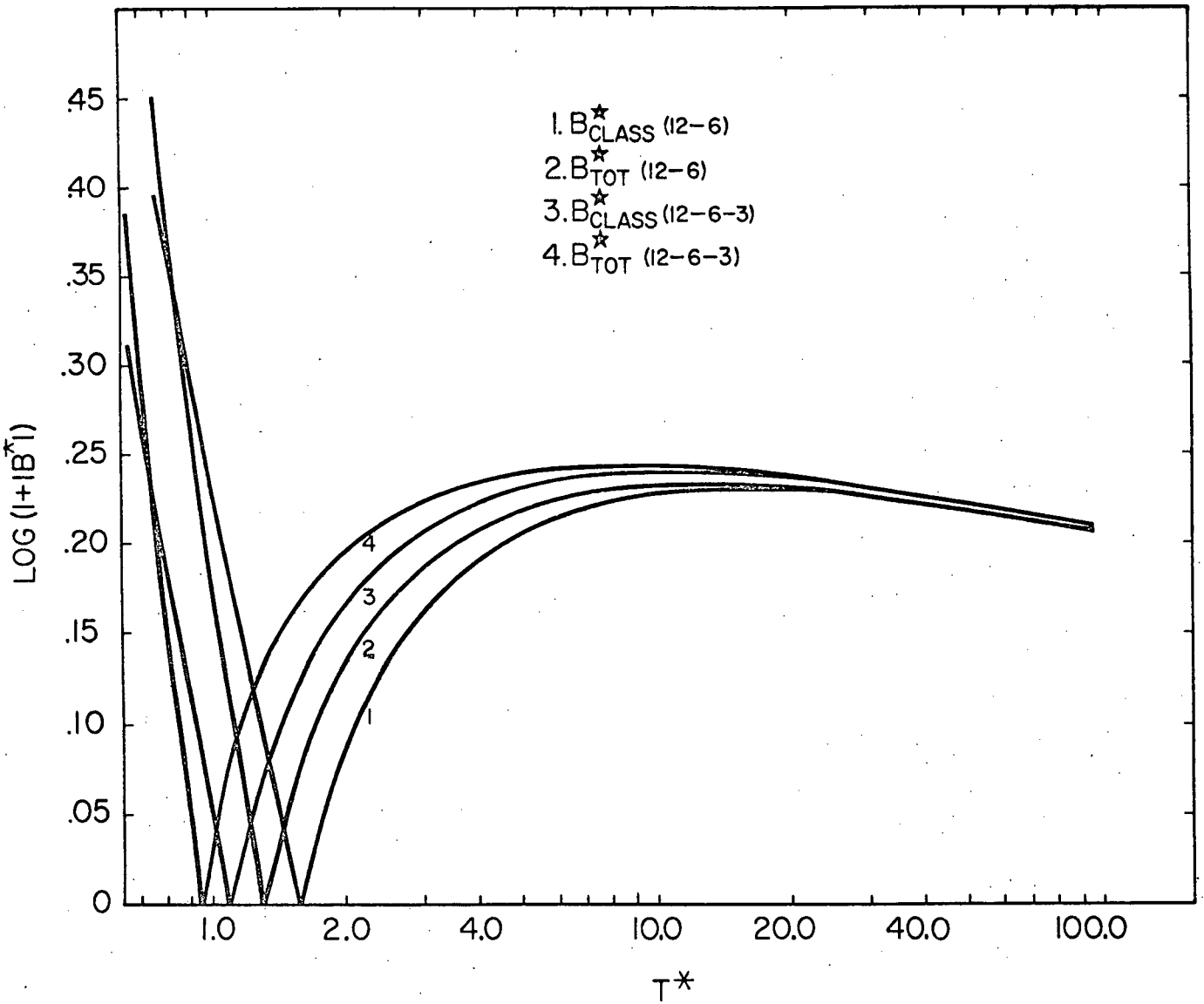
1. B^{*}_{CLASS} (12–6)
2. B^{*}_{TOT} (12–6)
3. B^{*}_{CLASS} (12–6–3)
4. B^{*}_{TOT} (12–6–3)
LOG (1+|B*|)
.45
.40
.35
.30
.25
.20
.15
.10
.05
0
1.0
2.0
4.0
10.0
20.0
40.0
100.0
T*
1
2
3
4

deviations increase as the temperature is lowered and the quantum curves lie above the classical ones. The maximum quantum corrections occur in the vicinity of the classical Boyle points for the two models, which are at reduced temperatures of 1.56 and 1.11 respectively for (12,6) and (12,6,3) potentials. With further lowering of the temperature the net quantum corrections decrease and eventually become negative. Thus the quantum curves cross the classical ones and lie below them. For our hypothetical system one finds that the cross-over points occur at T^* values of 0.85 and 0.74 for the (12,6) and (12,6,3) models, respectively.

Owing to the fact that the Boyle temperature T_B^* depends quite strongly on n (see Appendix I), it is not really correct to make detailed comparisons between the models at identical values of T^*. It can be shown[12] for any n that ϵ_2/ϵ is in the same ratio as $T_B^*(12,6)/T_B^*(12,6,3)$, so that one should compare the models at corresponding values of reduced temperature relative to the Boyle point, i.e, at the same values of T^*/T_B^*. Figure 2 is a plot of $\log(1+|B^{(2)}\hbar|)$ versus relative reduced temperature, and the difference between the models is more obvious. It would appear from this figure that the quantum corrected curves differ more in shape than do the classical ones.

It is clear that at low temperatures the Wigner-Kirkwood expansion to $\hbar^4$ no longer converges and the present treatment breaks down. We wish to show that one can establish reliable limits within which the treatment used here can be applied. However, it should be noted that the following discussion applies only to the Wigner-Kirkwood expansion to order $\hbar^4$.

FIGURE 2

Reduced two-dimensional second virial coefficient in classical and Bose-Einstein quantum statistics as a function of relative reduced temperature. Comparison of (12,6) and (12,6,3) potentials for HBEG.

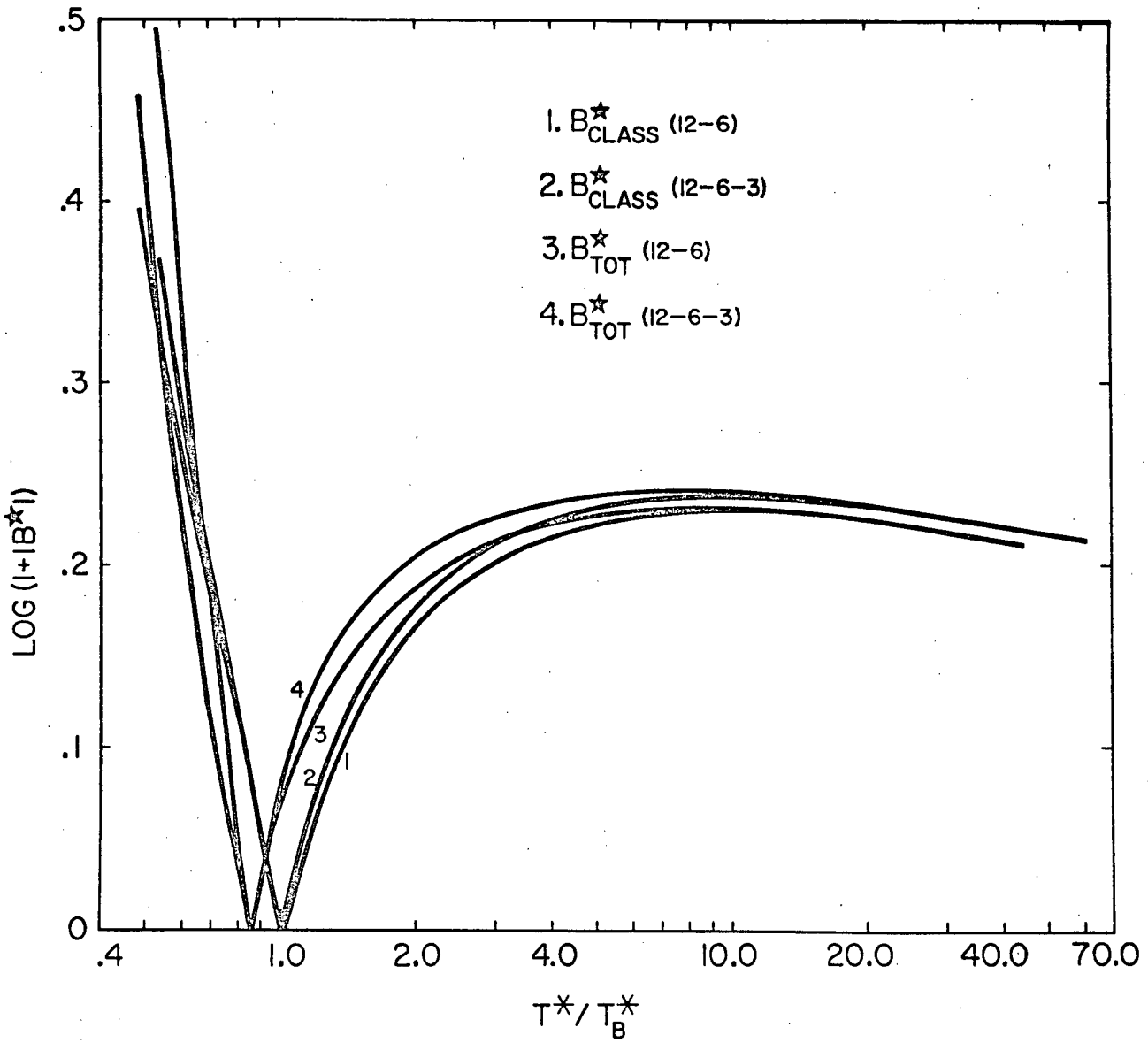
.5
.4
.3
.2
.1
0
LOG (1+|B*|)
1. B*CLASS (12-6)
2. B*CLASS (12-6-3)
3. B*TOT (12-6)
4. B*TOT (12-6-3)
4
3
2
1
.4
1.0
2.0
4.0
10.0
20.0
40.0
70.0
T*/T*B

Although recursion formulas[21,25] have been presented to calculate higher order terms, the amount of work involved is extremely tedious. For this reason all previous second virial coefficient studies using the Wigner-Kirkwood expansion have been truncated at the $\hbar^4$ term. Therefore our discussion of the convergence of this series is of a practical nature only, and in no way describes the convergence properties of the complete untruncated expansion.

There are two criteria for physical reasonable quantum deviations which can be used to set such limits. Firstly, for any value of the quantum parameter Λ^*, $B^{(2)*} - B_{cl}^{(2)*}$ should be positive and monotonically increasing with decreasing temperature. From Figures 1 and 2 it is obvious that this criterion is not met on the attractive branch for either model, but that $B^{(2)*} - B_{cl}^{(2)*}$ exhibits a maximum and then declines. In order to use this criterion to set a low-temperature limit for the treatment, one must solve the equation

$$[\partial(B^{(2)*} - B_{cl}^{(2)*}) / \partial T^*]_{\Lambda^*,n} = 0 \quad , \tag{4.01}$$

which requires a computation of the temperature derivatives of $B_l^{(2)*}$, $B_{ll}^{(2)*}$ and $B_{perf}^{(2)*}$. The algebra is straight-forward but formidable in quantity, especially for the (12,6,3) potential, where the calculations must be repeated for every n value of interest. Moreover, we feel that (4.01) probably sets too low a limit, for a reason mentioned below. It would probably be safer to use the expansion only down to the point

$$[\partial^2 (B^{(2)*} - B_{cl}^{(2)*}) / \partial T^{*2}]_{\Lambda^*,n} = 0, \tag{4.02}$$

and the labour would be further increased (e.g., the second derivative of $B_l^{(2)*}$ for the (12,6,3) model involves the evaluation of 30 integrals).

However, there is a second criterion which is considerably simpler and appears to set a bound lying between those given by (4.01) and (4.02). That is, at fixed T^*, the quantum deviations should be a monotonically increasing function of Λ^*. But if one plots $B^{(2)*}-B_{cl}^{(2)*}$ versus Λ^* at constant T^* it is again found that a maximum exists at some value $\Lambda^*_{max,}$, which can be determined through

$$[\partial(B^{(2)*} - B_{cl}^{(2)*}) / \partial\Lambda^*]_{T^*,n} = 0, \qquad (4.03)$$

whence, for the two-dimensional gas,

$$\Lambda^*_{max} = [(B_{perf}^{(2)*} - B_l^{(2)*}) / 2B_{ll}^{(2)*}]^{1/2}_{T^*,n} . \qquad (4.04)$$

Λ^*_{max} has the physical significance that for any T^* there exists an upper bound on the quantum parameter such that the quantum corrections are monotonic in Λ^*. One can therefore construct a curve of the the type shown in Figure 3, plotting relative reduced temperature against Λ^*_{max}. Such a curve can be thought of as giving the radius of convergence in the plane $(T^* / T_B^*, \Lambda^*)$, since for all points lying within the area bounded by the ordinate and the curve, the Wigner-Kirkwood expansion to order $\hbar^4$ converges.

As seen in equation (4.03) the radius of convergence is a function of η, and it is evident from Figure 3 that increasing η serves to decrease the convergence limits. As the curve for $\eta=0$ corresponds to the pure (12,6) potential, we can now say that for any value of Λ^* the quantum (12,6)

FIGURE 3

Radius of convergence of the WK expansion in two and three dimensions. Curve 1, two-dimensional (12,6,3) potential with $n = -0.05$. Curve 2, two-dimensional (12,6) potential. Curve 3, three-dimensional (12,6) potential.

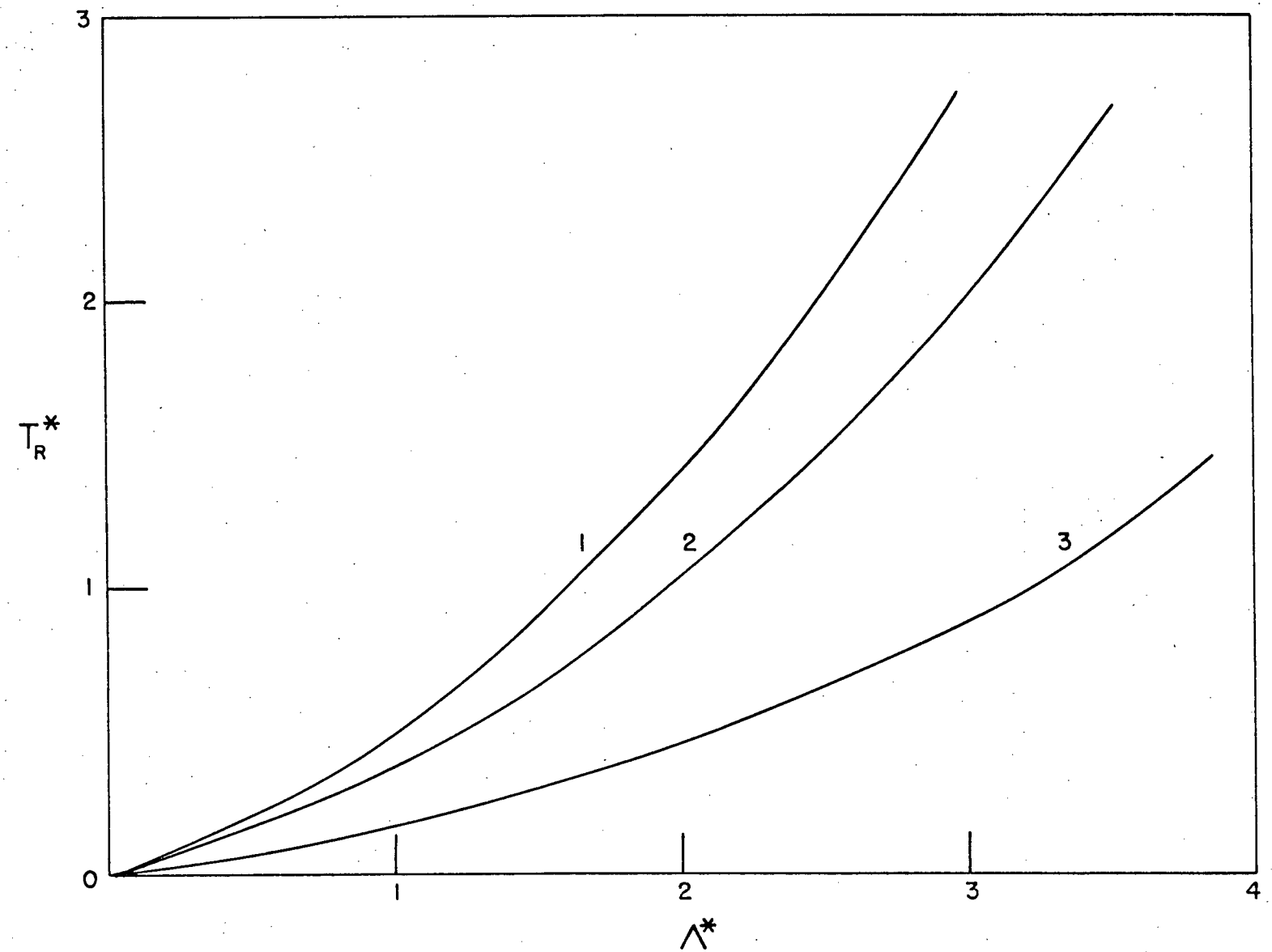
3
2
1
0
T_R^*
1
2
3
1
2
3
4
Λ^*

model is applicable over a wider range of temperatures than is the (12,6,3). Similarly, at a given temperature the (12,6) model can accomodate the more degenerate case. This observation is modified to some extent by the fact that the parametric renormalization required for the (12,6) potential invariably increases the value of Λ^*. This increase may or may not be sufficient to offset the difference in models, depending upon the η value required. For example, at the Boyle point the (12,6) model can be used for $\Lambda_2^* \leq 2.0$, while the (12,6,3) model with $\eta=-0.05$ is only applicable for $\Lambda^* \leq 1.6$ so that the (12,6) potential can be used for HBEG at this temperature whereas the (12,6,3) cannot. However, the (12,6,3) case is convergent at this temperature for HBEG so long as $|\eta| \leq 0.03$.

To investigate more fully the dependence of the quantum corrections on η, we have constructed for our hypothetical gas curves of $B^{(2)*} - B_{cl}^{(2)*}$ versus T^*/T_B for differance values of η. (See Figure 4). The dependence of the convergence limit on this parameter is evident from the shift in the position of the maximum. We should mention that in all cases the temperature limit of convergence found from Figure 3 lies to the right of the corresponding maximum in Figure 4, and appears to be slightly to the left of the inflection point. It should now be clear why we feel equations (4.02) and (4.03) provide more realistic convergence limits than does equation (4.01). This is brought out even clearer by comparing curves 1 and 3 in Figure 4, the difference here being caused only by different Λ^* values. At the intersection of these curves, which lies on the high temperature side of both maxima, we have the very unreasonable situation of the

FIGURE 4

Dependence of the quantum corrections to the two-dimensional second virial coefficient on the perturbational parameter η. Curves 1,2,4,5, are for the (12,6,3) potential with $-\eta$ values of 0,0.01,0.03,0.05, respectively. Curve 3 is for the (12,6) potential.

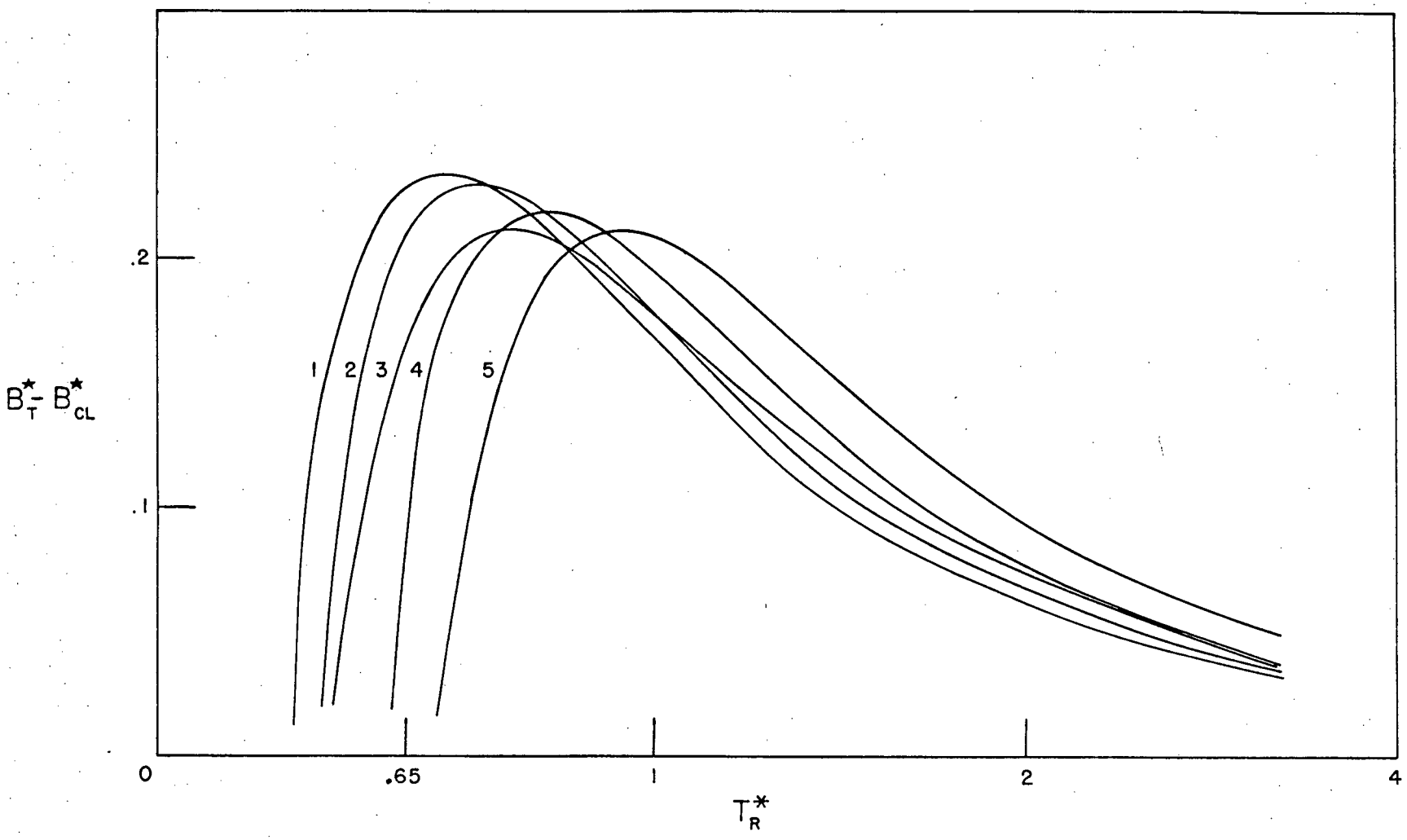
$B_T^* - B_{CL}^*$
.2
.1
1
2
3
4
5
0
.65
1
2
4
T_R^*

same potential function yielding the same net quantum corrections at the same temperature for two different values of Λ^*.

In the region where the $\hbar^4$ expansion converges, $B^{(2)*} - B_{cl}^{(2)*}$ increases monotonically with $|\eta|$ at any relative reduced temperature, so that the larger the perturbation by the field the more the quantum defects will be enhanced. However, the question of which potential model predicts the large quantum deviations at a given temperature is difficult to answer, the situation being complicated by two competing effects. On the one hand, as $|\eta|$ increases the corrections for the (12,6,3) potential are enhanced, but on the other hand this increase in the perturbation will also serve to increase the corrections for the (12,6) potential, since as the magnitude of the perturbation increases, ε_2 decreases and there is a concomitant rise in Λ^*_2. It therefore appears that in order to say which model will produce the larger quantum deviations one must know both η and Λ^*_2, which effectively precludes an a priori estimate.

Concerning the effect of reducing the dimensionality of the problem, Figure 5, showing the classical and Bose-Einstein quantum curves, for $B^{(3)*}$, $B^{(2)*}$, $B^{(1)*}$ as functions of reduced temperature, provides a striking comparison. These curves are computed for hydrogen molecules interacting via a (12,6) potential. As the dimensionality of the problem decreases the relative reduced temperature increases at which a treatment of the $\hbar^4$ expansion fails. In three dimensions the treatment appears to be satisfactory down to a relative reduced temperature as low as 0.4, whereas in two dimensions below about 0.9 the quantum corrections begin to decrease

FIGURE 5

Second virial coefficient in one, two, and three dimensions. In each case, curve 1 is the Bose-Einstein quantum curve for HBEG, and curve 2 is for a classical gas.

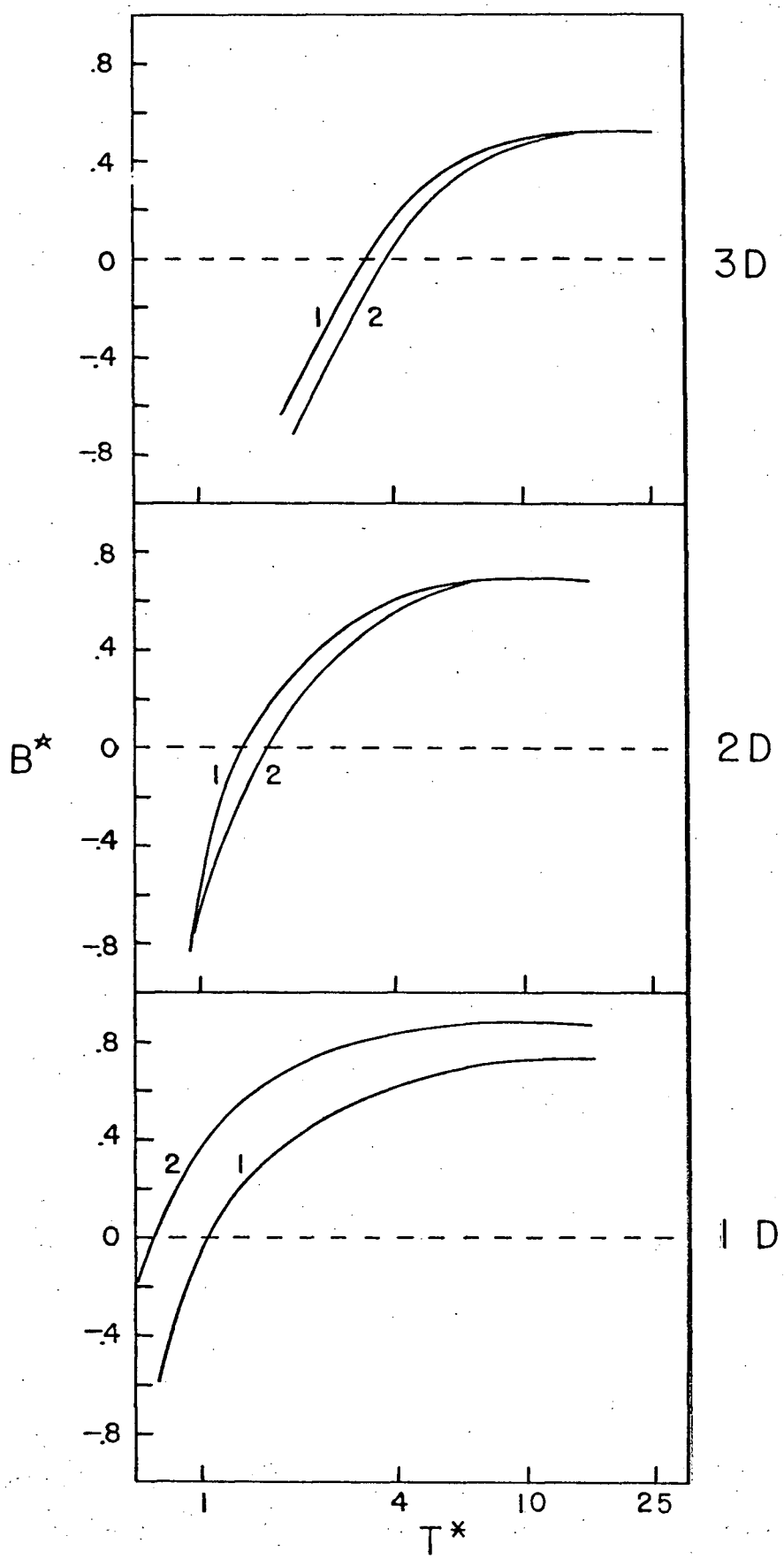
.8
.4
0
-.4
-.8
1
2
3D
B*
2D
1D
1
4
10
25
T*

with decreasing temperature and the curves eventually cross. Note that in one dimension[36] there appears to be no temperature at which the treatment is satisfactory, the net quantum corrections being always negative.

As was done in two-dimensions, we can calculate for the three-dimensional case the value of Λ^* at which the quantum correction cease being monotonic is Λ^* at any given temperature. In this case we find

$$\Lambda^*_{max} = [3B_{perf}^{(3)*} + (9B_{perf}^{(3)*2} - 32B_{I}^{(3)*}B_{II}^{(3)*})^{1/2}]/8B_{II}^{(3)*} \quad (4.05)$$

Using the tabulations of Hirschfelder, Curtiss and Bird[23] we can then construct a radius of convergence curve for the three-dimensional (12,6) gas, having employed a Wigner-Kirkwood $\hbar^4$ expansion for the quantum corrections. This has been included in Figure 3, from which it is apparent that the three-dimensional results are usable over a much wider range than the two-dimensional ones. When the one-dimensional results are examined it is found that there is no value of Λ^* which leads to positive quantum corrections at any temperature whatever.

If one compares, at a fixed relative reduced temperature, the terms which make up the Wigner-Kirkwood quantum corrections to order $\hbar^4$, one finds that, as the dimensionality of the gas decreases, the magnitude of each contribution increases, with B_{II}^* increasing relatively more than B_I^*. For example, at a relative reduced temperature of about 7, the following ratios are found: $B_I^{(3)*} : B_I^{(2)*} : B_I^{(1)*} \sim 1:2:3$; and $B_{II}^{(3)*} : B_{II}^{(2)*} : B_{II}^{(1)*} \sim 1:6:20$. Of course, the differences are even larger at lower temperatures. The net effect is that the series expansion to order $\hbar^4$ diverges in one and two dimensions at temperatures, where it is

still quite rapidly convergent in three domensions.

From another point of view, equation (3.23) can be regarded as a development in powers of the operator $\underset{\sim}{\nabla}$. Hence the requirement for convergence of the series is that the differential quotients of ϕ are small compared to ϕ, and that the higher orders become successively smaller. Clearly, this requirement is met less and less satisfactorily as the dimensionality is reduced.

However, the real "offender" in the lower-dimensional cases is the perfect gas contribution, owing largely to the altered temperature dependence:

$$B_{perf}^{(3)\star} \propto T^{*-3/2} \; ; \; B_{perf}^{(2)\star} \propto T^{*-1} \; ; \; B_{perf}^{(1)\star} \propto T^{*-1/2}.$$

Thus for two-dimensional and especially one-dimensional gases, the effects due to symmetry of the wave functions fall off rather slowly with increasing temperature. In fact, for the one-dimensional gas, $B_{perf}^{(1)\star}$ dominates over the Slater sum contributions at all temperatures above $T^{*} \sim 0.6$, while below this temperature the Wigner-Kirkwood expansion to order $\hbar^4$ is everywhere divergent. The following comparison is instructive. In the vicinity of the Boyle point, $B_{perf}^{(3)\star} : B_{perf}^{(2)\star} : B_{perf}^{(1)\star} \sim 1:20:450$, while at a relative reduced temperature of about 7 the corresponding ratios are $\sim 1:50:3000$.

CHAPTER 5

ANALYSIS OF THE DATA

TWO-DIMENSIONAL SECOND VIRIAL COEFFICIENT

We have seen that one can determine experimentally the ratio of $B^{(2)}/A$ from the intercept and initial gradient of a plot of $\bar{N}a/p$ versus p. It was shown in Chapter 3 that for the (12,6,3) model one has the theoretical form

$$B^{(2)*} = f(T^*, n, \Lambda^*). \qquad (5.01)$$

For any given system ϵ and σ, hence Λ^*, are fixed, so that a comparison of the temperature dependence of $B^{(2)}/A$ with the theoretical curve of $B^{(2)*}$ versus T^* yields "best-fit values" of the parameters n and Λ^*. By "best-fit values", we mean those values of the fitting parameters which minimize the standard deviation between the experimental points and the theoretical curve, i.e., one proceeds by finding that value of n which minimizes the standard deviation in A. This fitting procedure is quite analogous to that used in determining force constants from gas phase virial coefficient data.

In the case of the renormalized (12,6) function,

$$B^{(2)*} = f(T_2^*, \Lambda_2^*), \qquad (5.02)$$

$$T_2^* = kT/\epsilon_2, \quad \Lambda_2^* = h/\sigma_2 (m\epsilon_2)^{1/2}. \qquad (5.03)$$

The fitting procedure now is a bit more complicated. One first fits the $B^{(2)}/A$ versus T data to $B_{cl}^{(2)*}$ versus T^* to obtain a first estimate of the parameters ϵ_2 and $A^* = A/\frac{1}{2}\pi N \sigma_2^2$. From σ and the ratio ϵ/ϵ_2, σ_2 can be computed from (3.50) and an estimate of Λ_2^* obtained. The data are

now refitted to the full quantum corrected curve of $B^{(2)*}$ versus T^*, commencing a series of successive approximations to consistent values of ε_2, σ_2, Λ_2^* and A. Note from the form of the (12,6,3) potential in equation (1.20), that once η is known one can obtain the effective well depth ε_2, the collision diameter σ_2, and the position of the potential minimum τ_o for this model:

$$\phi(\sigma_2) = 0 \tag{5.04}$$

$$\phi(\tau_o) = -\varepsilon_2, \tag{5.05}$$

$$\left(\partial\phi/\partial\tau\right)_{\tau_o} = 0. \tag{5.06}$$

Hence, for both models one can estimate the perturbation of the gas-gas pair potential by the field from a comparison of the effective parameters with those of the bulk gas.

In this connection it should be mentioned that the η values found using the (12,6,3) potential and thus the effective parameters, are quite strongly influenced by one's choice of bulk gas force constants.[12] A variation in the bulk-gas parameters will affect the results in the following ways. Firstly, the experimental $B^{(2)}/A$ values will change slightly owing to differences in the corrections for bulk gas imperfections which must be applied to the C_{AAS} data. Secondly, the two fitting parameters η and A will vary, both by virtue of the altered $B^{(2)}/A$ values and because of their inherent dependence upon ε/k and σ; η is primarily dependent upon the energy parameter, and A upon the collision diameter, although there is also some slight interdependence. Therefore, this limitation

should be kept in mind in discussing the significance of the results.

For CH_4 we have used the bulk gas parameters given by Michels and Nederbragt[37]:

$$CH_4 : \quad \varepsilon/k = 148.2\,^{\circ}K , \quad \sigma = 3.82\,^{\circ}A.$$

The energy parameter for CD_4 has been taken to be 0.9% lower than that for CH_4, in order to agree with the findings of Thomaes and van Steenwinkel[38]. However, we have retained the same σ values for both gases, as the difference in this parameter between CH_4 and CD_4 has not been reliably determined and in any case should be quite small. Thus, the CD_4 bulk gas parameters used are:

$$CD_4 : \quad \varepsilon/k = 146.9\,^{\circ}K , \; \sigma = 3.82\,^{\circ}A.$$

For H_2 and D_2, we have used the values found by Michels, et.al.[19]:

$$H_2 : \quad \varepsilon/k = 36.7\,^{\circ}K , \quad \sigma = 2.959\,^{\circ}A$$

$$D_2 : \quad \varepsilon/k = 35.2\,^{\circ}K , \quad \sigma = 2.952\,^{\circ}A.$$

These values are the best fit quantum parameters. For the classical parameters, those values found by Michels and Goudeket[39,40] are used:

$$H_2 : \quad \varepsilon/k = 29.2\,^{\circ}K , \quad \sigma = 2.87\,^{\circ}A$$

$$D_2 : \quad \varepsilon/k = 31.1\,^{\circ}K , \quad \sigma = 2.87\,^{\circ}A.$$

Table I presents the results of the present analysis of data[41] for CH_4 and CD_4 interacting with graphite, together with the previously determined classical results[12,27], which have been included for purposes of comparison. For both potential models it is seen that the quantum corrections are quite small (as was anticipated), amounting to no more

Table I. Curve fit results for two-dimensional CH_4 and CD_4 on graphite.

	(12,6) Potential				(12,6,3) Potential				
Molecule	ε_2/k(°K)	σ_2(Å)	Λ_2^*	Std. dev.	ε_2/k(°K)	σ_2(Å)	Λ^*	-n	Std. dev.
				1. Classical Fit					
CH_4	129.2	3.86		0.425	139.2	3.84		0.0216	0.433
CD_4	129.3	3.86		0.428	138.6	3.84		0.0201	0.435
				2. Quantum Fit					
CH_4	129.8	3.86	0.244	0.424	139.5	3.84	0.231	0.0208	0.431
CD_4	129.8	3.86	0.222	0.426	138.8	3.83	0.211	0.0194	0.433

than 0.5% of the pair interaction energy. These corrections are larger for the (12,6) potential than for the (12,6,3). In Chapter 4 it was pointed out that it seemed impossible to determine a priori which model would yield the larger corrections in any given case because of two competing effects. At the same relative reduced temperature, the quantum deviations increase with increasing $|\eta|$, but on the other hand the (12,6) model appears always to provide the larger Λ^* value. Hence, each case will differ, depending on the difference in Λ^* values and on the magnitude of η.

Note that the best-fit value of $|\eta|$ decreases by about 4% with the introductions of the quantum corrections. Since η is a measure of the perturbation of the gas phase potential by the field, this reduction is then reflected in the slightly increased effective interaction energies. However, these effective energies are quite insensitive to changes in η, rising by only about 0.2%.

Unfortunately, the change in standard deviation of the fit when the quantum defects are included is essentially the same for both models, so that it is still impossible to make any definitive choice. This of course owes to the fact that the deviations from classical behaviour are very small. We have not included values of the other fitting parameter, A, in Table I , as they are effectively unchanged from the classical results which have been discussed elsewhere.[12,27]

From the bulk gas and effective two-dimensional parameters we can calculate the apparent nonadditivity induced in the pair interaction by the surface field. Table II lists values of the quantity $\Delta = (\varepsilon - \varepsilon_2)/\varepsilon$.

Table II.

Values of $\Delta=(\varepsilon-\varepsilon_2)/\varepsilon$ and $\delta_2=[\varepsilon_2(H)-\varepsilon_2(D)]/\varepsilon_2(D)$ for CH_4 and CD_4 based on the four models.

Model	Molecule	$\Delta \times 10^2$	$\delta \times 10^2$
CI(12,6)	CH_4	12.8	-0.1
	CD_4	12.0	
CI(12,6,3)	CH_4	6.1	±0.4
	CD_4	5.7	
Q(12,6)	CH_4	12.4	±0.0
	CD_4	11.6	
Q(12,6,3)	CH_4	5.9	±0.5
	CD_4	5.5	

It is clear from these values that one could draw rather different conclusions concerning the magnitude of the perturbation on the basis of the different models, since the effect for the (12,6) potential is 2.1 times that shown by the (12,6,3). However, the small change indicated by the (12,6,3) values probably should not be taken too seriously for the following reason. If one applies a (12,6) model to both the bulk phase and the two-dimensional layer, the shape of the potential wells will be the same and the entire perturbation must be absorbed in changing just the depth of the well and the position of the minimum. But introduction of the inverse cube term appreciably alters the shape of the potential curve, and this apparently means that the well depth does not have to change to the same extent.

We have pointed out that a different choice of bulk parameters would change the values given in Table II, but we can state with reasonable assurance that it would not alter the significance of the results. An examination of the results for Ar, Kr and Xe[12] reveals an interesting coincidence. For each of these gases, four different sets of bulk potential parameters were employed in the analysis, which led to four values of n, ε_2 and Δ. Yet in every case the ratio $\Delta(12,6)/\Delta(12,6,3)$ for a given ε turn out to be 2.11 ± 0.02. Why this should be so is not readily apparent, but the results seem too general to be entirely fortuitous.

It is interesting that for both models the Δ values for CD_4 are 6-7% lower than those for CH_4. This would indicate that for the lighter molecule the pair interaction is more strongly perturbed. This seems entirely reasonable on two accounts. Firstly, there is a polarizability difference of 1.45% between the isotopes[17], that for CD_4 being the lower.

Presumably, the less polarizable a molecule, the less it will be perturbed by the external field. Secondly, the gas-solid interaction energy is $\sim$ 1.2% greater for CH_4 than for CD_4[20] (see Table VI).

Finally we should comment on the values of $\delta=[\varepsilon_2(H) - \varepsilon_2(D)]/\varepsilon_2(D)$ appearing in Table II. Whereas the (12,6) model suggests that this quantity is effectively nil, the (12,6,3) values give an indication of a definite change in ε_2 with deuterium substitution. For the methanes in three-dimensions[38], $\delta = +0.9\times10^{-2}$, so the effect in two dimensions appears to be only about half that found in three, although the signs are the same. Yaris[10] has derived a theoretical expression for the difference $\varepsilon - \varepsilon_2$, which may be used together with values of ε to calculate δ. This provides the estimate $\delta = +0.4\times10^{-2}$, in good agreement with the (12,6,3) values.

The B_{AS}, C_{AAS}, and $B^{(2)}/A$ values for H_2 and D_2 on graphite are computed from the isotherms of Constabaris, et.al.[41] are given in Table III. From the $B^{(2)}/A$ values for H_2 it is obvious that the data are very scattered, since this quantity should be a monotonically increasing function of temperature. This explains the unreasonable best fit ε_2/k values for the (12,6) potential:

classical : $\varepsilon_2/k = 54.0^{\circ}K$

quantum : $\varepsilon_2/k = 63.5^{\circ}K$.

These values imply an enormous additional attraction between H_2 molecules due to the presence of the field created by the surface. This attraction implies multilayer adsorption but in the temperature region of the data, one has monolayer adsorption since the adsorbed phase is about 6% of the monolayer coverage. Therefore the assumption that there could be co-operative adsorption is unreasonable.

Table III

B_{AS} and C_{AAS} data for H_2 and D_2 adsorbed on P33 (2700°)

	HYDROGEN			DEUTERIUM		
T	B_{AS}	$-C_{AAS}$	$B^{(2)}/A$	B_{AS}	$-C_{AAS}$	$B^{(2)}/A$
90.057	.4245	1218.68	6763.88	.4380	1111.02	5792.06
97.122	.2853	610.599	7501.58	.2927	550.884	6428.74
104.156	.2014	322.071	7940.22	.2093	340.784	7781.53
109.903	.1554	182.936	7575.25	.1590	171.107	6772.46
117.049	.1183	117.761	8413.15	.1206	106.054	7296.60
124.128	.0928	73.867	8586.63	.0938	63.902	7269.08
131.069	.0724	31.734	6055.75	.0752	44.309	7826.98
138.128	.0605	15.175	4144.52	.0614	29.503	7818.17

A plot of log C_{AAS} versus 1/T should be nearly linear, but when this criterion is applied to the H_2 data it is found that the two highest temperature points deviate widely. We have therefore refitted these data using six points only (131°K and 138°K omitted).

The D_2 data were analysed using all 8 data points. Although the log C_{AAS} versus 1/T plot for these data showed considerable scatter, there was no firm basis for preferentially omitting one or more points. Table IV contains the results of the fits for the two-dimensional (12,6) model for H_2 and D_2 on P33 (2700°). Error limits on the ε_2/k values have been established by applying the estimated experimental uncertainties[9] to the original isotherm data, computing new B_{AS} and C_{AAS} values, and fitting these to the model. These results indicate the ε_2/k values are uncertain to $\pm$ 1.0°K for H_2 and $\pm$ 1.4°K for D_2.

Several remarks should be made here regarding the values presented in Table IV. To begin with, the quantum effects for H_2 are considerably larger than those for D_2. If one calculates $\rho = (\varepsilon_Q - \varepsilon_{cl})/\varepsilon_Q$ for both gases, one finds that $\rho_H/\rho_D = 1.74$. Classically, the two gases yield essentially the same interaction energy. However, when quantum effects are included, hydrogen appears to have the larger ε_2 value. This inverse effect is to be expected on the basis of the polarizability difference between the isotopes. The surface area values obtained are in good agreement with those found from a similar analysis of data for the rare gases adsorbed on this surface, which lie in the range 9.5 - 11 m^2g^{-1}. Comparing the standard deviations in Table IV, the H_2 data fit significantly better than those for D_2. This was anticipated from the greater scatter in the D_2 C_{AAS} values.

Table IV

Curve fit results for two-dimensional (12,6) H_2 and D_2 on graphite

Molecule	$\epsilon_2/k(°k)$	$\sigma_2(\mathring{A})$	$A(m^2g^{-1})$	Λ_2^*	Std.dev.
		1. Classical fit			
H_2	31.0	3.001	11.0		.21
D_2	32.0	2.976	12.0		1.26
		2. Quantum fit			
H_2	37.0	2.957	10.7	1.714	.21
D_2	35.5	2.950	11.8	1.240	1.26

Table V contains values of $\Delta = (\varepsilon-\varepsilon_2)/\varepsilon$ and $\delta_2 = (\varepsilon_2(H) - \varepsilon_2(D))/\varepsilon_2(H)$ for the (12,6) potential. Also included for comparison are the three-dimensional δ values. The Δ values in Table V are zero within experimental error. Both classically and quantally, the uncertainties in δ_2 are sufficiently large that this quantity could have either sign, although it is likely to be positive for the quantum corrected fit.

A (12,6,3) analysis for hydrogen and deuterium has been attempted but again the results are ambiguous. The experimental uncertainties are such that η, which is very small ($|\eta| \lesssim 0.01$), could be either positive or negative. Hence we have not included the results for this model. It is disappointing that these analyses of the data for the hydrogen isotopes have provided so little information. Any definitive analysis of the two-dimensional (12,6) and (12,6,3) models will have to wait until more reliable data have been obtained.

SECOND GAS-SURFACE VIRIAL COEFFICIENT

Here we analyse the data[16] of H_2, D_2, CH_4 and CD_4 on P33 (2700°) by fitting the experimental B_{AS} values to the quantum corrected theoretical expression for the second gas-surface virial coefficient. Three different models for the interaction potential were used, the (9.3), (10,4), and (12,3). The fitting procedure used was to compare the temperature dependence of the experimental B_{AS} values with the theoretical quantum expression (3.52). In the work of Constabaris, et.al.,[16] data for B_{AS} as a function of temperature were fitted to B_{AS}^{cl}* by adjusting the two parameters ε_{1s}/k and Az_o,

Table V

Values of $\Delta = (\varepsilon-\varepsilon_2)/\varepsilon$ and $\delta_2 = (\varepsilon_2(H) - \varepsilon_2(D))/\varepsilon_2(H)$ for the two-dimensional (12,6) H_2 and D_2.

Model	Molecule	$\Delta\times10^2$	$\delta_2\times10^2$	$\delta\times10^2$
Cl(12,6)	H_2	-6.2 ± 3.4		
			-3.2 ± 7.6	-6.5
	D_2	-2.9 ± 4.5		
Q(12,6)	H_2	$-.82\pm2.7$		
			$+4.1\pm6.2$	+4.08
	D_2	$-.85\pm4.0$		

thus obtaining best-fit values for these parameters. One then calculates z_o as described below, and a classical estimate of Λ_s^*. The B_{AS} values are then fitted to the quantum corrected gas-surface virial coefficient, where

$$B_{AS} = f(T^*, \Lambda_s^*), \tag{5.07}$$

$$T^* = kT/\epsilon_{ls}, \quad \Lambda_s^* = h/z_o(m\epsilon_{ls})^{1/2}. \tag{5.08}$$

One again finds best-fit values for ϵ_{ls}/k and Az_o, and calculates a new Λ_s^* value. This process is repeated until one obtains self-consistent ϵ_{ls}/k, Az_o and Λ_s^* values.

The principal difficulty in the analysis of second-order interaction data lies in the evaluation of the apparent gas-surface collision diameter z_o. Not only must this quantity be known to obtain the apparent surface area, but also, as seen from (3.52) and (5.08), the quantum corrections will depend strongly on the exact value of z_o. In the past[20], the gas-surface attractive potential has been identified with the London forces attraction of two isolated systems,

$$\epsilon_{ij} = C/r_{ij}^6 . \tag{5.09}$$

C, the constant of proportionality, has been evaluated by means of the Kirkwood-Muller formula,

$$C_{KM} = (6m_e c^2 \alpha_1\alpha_2)[\alpha_1/\chi_1 + \alpha_2/\chi_2], \tag{5.10}$$

where the α's and the χ's are polarizabilites and diamagnetic susceptibilities,

respectively, of the molecules, m_e the electronic mass, and c the velocity of light. In addition to following the above procedure, two other equations are also employed here for calculating C. The first is due to Slater and Kirkwood[44,45],

$$C_{SK} = (3e\hbar/2m_e^{1/2})\alpha_1\alpha_2 [1/\{(\alpha_1/n_1)^{1/2} + (\alpha_2/n_2)^{1/2}\}], \quad (5.11)$$

and the second due to London[44,45],

$$C_L = (3\alpha_1\alpha_2 I_1 I_2) / 2(I_1+I_2) . \quad (5.12)$$

In (5.11) and (5.12), e is the electronic charge, the I's the ionization potentials and the n's the number of electrons in the outer shell of the molecules.

Comparing one of the C values with the experimental values of ϵ_{ls} then gives z_o. For the (9,3) and (12,3) models, equation (5.09) and the generalized Lennard-Jones potential,

$$\phi(r) = (n/(m-n))(n/m)^{m/(n-m)} \varepsilon[(r_o/r)^n - (r_o/r)^m], \quad (5.13)$$

must be consistent at large separations. One therefore identifies

$$C = (n/(m-n))(n/m)^{m/(n-m)} \varepsilon r_o^n \quad (5.14)$$

Then integrating (5.09) over a semi-infinite solid yields

$$\epsilon_{ls} = \frac{-N_o C}{6z_o^3} [\beta(\beta-\alpha)(\beta/\alpha)^{\alpha/(\beta-\alpha)} - 1], \quad (5.15)$$

where, again, α=n-3 and β= m-3 for the (9,3) potential, α=n and β=m-3 for the (12,3) potential and N_o is the number of atoms per cm^3. in the

solid. For the (10,4) model, integration of (5.09) over a single infinite plane results in the expression

$$\epsilon_{ls} = -N_o^{I} C/2z_o^4 \quad , \tag{5.16}$$

and so for this potential,

$$\epsilon_{ls} = \frac{-N_o^{I} C}{2z_o^4} \left[\beta(\beta-\alpha) \, (\beta/\alpha)^{\alpha/(\beta-\alpha)} \right]^{-1} , \tag{5.17}$$

where $\alpha = n-2$, $\beta = m-2$, and N_o^{I} is the number of atoms per cm^2. of the surface.

The parameters of best fit are presented in Tables VI and VII. It is seen that the quantum statistical mass corrections have the effect of reversing the order of interaction energies with the hydrogen isotopes. That is, when the mass effect on the vibrational levels normal to the surface are taken into account, one finds that the lighter isotope exhibits a slightly stronger interaction with the surface. Olivier and Ross[46] have made a harmonic oscillator zero-point energy approximation for the mass corrections, using the data employed here, and find the same order of isotopic interaction. However, these authors failed to consider the cause of this difference in interaction energy for isotopic pairs, and thus did not explain the reversal in the amount of gas adsorbed between the hydrogen and methane pairs. As we have seen, this reversal is brought about by the quantum mechanical effect of isotopic substitution on the dispersion forces, which serves to increase the attractive potential of the hydrogen substituted species. This effect is large enough in the case of the methanes, to cancel out the small mass effect, and thus CH_4 is adsorbed more readily

Table VI

Comparison of classical and quantum fit results using the Kirkwood-Muller Formula, Note: $\delta_s = [\varepsilon(H)-\varepsilon(D)]/\varepsilon(H)$,

Gas	$\varepsilon_{ls}/k(^\circ K)$		$A(m^2g^{-1})$		$z_o(\AA)$		Std.dev.(10^9)		$\delta_s(10^2)$
	Cl	Q	Cl	Q	Cl	Q	Cl	Q	
				(9,3) potential					
H_2	578	647	12.5	9.53	2.081	2.004	.705	.197	5.72
D_2	581	610	12.5	11.2	2.076	2.043	.521	.314	
CH_4	1450	1462	10.9	10.7	2.224	2.220	.186	.181	1.13
CD_4	1435	1444	11.1	11.0	2.231	2.228	.876	.854	
				(10,4) potential					
H_2	568	616	12.4	10.0	2.974	2.914	1.07	.509	3.73
D_2	571	593	12.4	11.3	2.969	2.941	.716	.517	
CH_4	1435	1441	10.5	10.4	3.120	3.117	.373	.363	1.25
CD_4	1418	1423	10.9	10.8	3.129	3.126	1.91	1.86	
				(12,3) potential					
H_2	579	679	13.5	9.07	2.226	2.112	.931	.199	8.72
D_2	582	619	13.6	11.8	2.222	2.177	.688	.341	
CH_4	1454	1462	11.7	11.6	2.379	2.375	.248	.240	1.16
CD_4	1438	1445	12.0	11.8	2.387	2.383	1.17	1.14	

Table VII

Quantum fit results using the Slater-Kirkwood (SK) and London (L) formulas.

Gas	ϵ_{ls}/k(°K)		A(m^2g^{-1})		z_o(Å)		Std. dev.(10^9)		δ_s(10^2)	
	SK	L	SK	L	SK	L	SK	L	SK	L
					(9,3) potential					
H_2	721		8.3		1.613		.305		13.2	
D_2	626		12.7		1.685		.517			
CH_4	1459	1462	12.4	14.5	1.910	1.621	.179	.178	1.17	1.23
CD_4	1442	1444	12.8	15.0	1.910	1.619	.849	.844		
					(10,4) potential					
H_2	638		10.6		2.522		.354		5.73	
D_2	601		12.5		2.553		.348			
CH_4	1442	1444	11.7	13.1	2.785	2.463	.362	.360	1.25	1.32
CD_4	1424	1425	12.1	13.6	2.785	2.461	1.85	1.84		
					(12,3) potential					
H_2										
D_2										
CH_4	1464	1468	13.4	15.6	2.042	1.733	.238	.235	1.16	1.23
CD_4	1447	1450	13.8	16.2	2.042	1.731	1.13	1.12		

than CD_4. Clearly, for two isotopes which are identical in every respect except their masses (eg. He^3 and He^4), the dispersion forces would be the same and the differences in adsorption properties could be explained solely by the quantum statistical mass effect. Thus, He^4 would be more readily adsorbed than He^3, owing to its lower lying position in the potential well.

As seen in Tables VI and VII, the mass corrections cause quite sizeable differences in the interaction energies and areas obtained for the hydrogen pair, but the differences are, of course, small in the case of the methanes. It is interesting to note that virtually all the change in ϵ_{ls}/k is due to the first quantum correction, B_{AS}^{I*}. When the hydrogen data are fitted to the (9,3) model omitting the B_{AS}^{II*} term, the interaction energy using the Kirkwood-Muller formula is found to be 649°K. This is due to the fact that Λ_s^* is small ($\approx$0.6), so that the higher terms contribute little. It should also be mentioned that the perfect term, B_{AS}^{perf*}, has no effect on the fit and therefore can be neglected.

The very large increase in the interaction energies when quantum corrections are included for the hydrogens is responsible for the impossibility of fitting the Slater-Kirkwood (12,3) model and all the London models for these gases, using the present computer programme. For $T^* \lesssim 0.125$, machine overflows prevent the calculation of B_{AS}^*. While this could be overcome by additional programming, it was felt that on the basis of the apparent areas found at these low T^*, the Slater-Kirkwood and London formulas would not yield particularly meaningful results in any case.

The area estimates obtained using the Kirkwood-Muller formula are in quite close agreement with those from the two-dimensional analysis, and lends further support to the use of this equation in the analysis of Henry's law adsorption data.

Of the three potential models examined, the (9,3) function seems to be the most successful as judged from goodness of fit, although the differences between the models are not as marked as had been hoped. The standard deviations for the (9,3) and (12,3) models are fairly similar, while that for the (10,4) is much worse. It is of interest to note that the quantum corrected fits for all the models are better than the classical ones. The differences are very small in the methanes, of course, since the quantum deviations are small. Methane fits all the models approximately five times better than tetradeutero-methane. For the hydrogens, the improvement in fit are quite apparent. The (10,4) model seems to fit the quantum corrected H_2 and D_2 equally well, whereas in all other cases, H_2 fits slightly better than D_2.

The percentage energy differences between isotopes in Tables VI and VII are not in the same order as the polarizability differences (1.32% and 1.45% respectively, for the hydrogens and methanes[17]). Moreover, the differences are much larger than one would expect on the basis of the gas phase values. If we assume the combining rule, $\varepsilon_{ls} \tilde{\nu} (\varepsilon_g \varepsilon_s)^{1/2}$ and use the measured[19,37] bulk gas Δ values, it follows that $[\varepsilon(H) - \varepsilon(D)] / \varepsilon(H)$ is 2.0% for the hydrogens and 0.41% for the methanes. Although this combining rule may not be especially accurate, it does not seem plausible that the difference

should be larger for the gas-surface case than for the bulk gas. It is felt this may indicate that the Wigner-Kirkwood expansion when applied to gas-surface interactions, and/or the model adopted for the solid are inadequate. Also if there is hindered rotation on the surface, as has been suggested[47], the use of a spherical potential may not be justified. We intend to examine these possibilities in the near future.

APPENDIX I

In this Appendix tables of $B^{(2)*}_{Cl}$, $B^{(2)*}_{I}$ and $B^{(2)*}_{II}$ are given at selected values of T^* and n for the (12,6,3) potential function. Also included is a table of $B^{(2)*}_{perf}$ values, which are of course independent of the potential. Note: $0.0^{3}2162 = 0.0002162$.

Table VIII-A

$-\eta = 0$

T^*	$B^{(2)*}_{Cl}$	$B^{(2)*}_{I}$	$-B^{(2)*}_{II}$
0.30	-14.127	15.412	21.793
0.40	- 6.4884	4.3959	3.8634
0.50	- 3.8113	1.9353	1.1866
0.60	- 2.5112	1.0726	0.49269
0.70	- 1.7578	0.68303	0.24667
0.80	- 1.2708	0.47640	0.14008
0.90	- 0.93193	0.35403	0.087025
1.00	- 0.68339	0.27555	0.057806
1.20	- 0.34469	0.18393	0.029452
1.40	- 0.12581	0.13407	0.017156
1.60	0.026518	0.10363	0.010955
1.80	0.13819	0.083493	$0.0^{2}74772$
2.00	0.22325	0.069367	$0.0^{2}53665$
2.50	0.36656	0.047865	$0.0^{2}27341$
3.00	0.45461	0.036009	$0.0^{2}16160$
3.50	0.51333	0.028620	$0.0^{2}10522$
4.00	0.55473	0.023622	$0.0^{3}73320$
5.00	0.60801	0.017356	$0.0^{3}40870$
6.00	0.63965	0.013627	$0.0^{3}25760$
8.00	0.67288	$0.0^{2}94419$	$0.0^{3}12752$
10.00	0.68778	$0.0^{2}71769$	$0.0^{4}75287$
15.00	0.69734	$0.0^{2}44389$	$0.0^{4}29904$
25.00	0.68771	$0.0^{2}24835$	$0.0^{5}98258$
50.00	0.65272	$0.0^{2}11633$	$0.0^{5}23181$
100.00	0.60557	$0.0^{3}55705$	$0.0^{6}57686$

Table VIII-B

$-\eta = 0.01$

T^*	$B^{(2)*}_{CI}$	$B^{(2)*}_{I}$	$-B^{(2)*}_{II}$
0.30	-12.766	13.906	19.406
0.40	- 5.8999	4.0630	3.5273
0.50	- 3.4574	1.8153	1.1001
0.60	- 2.2622	1.0163	0.46160
0.70	- 1.5666	0.65185	0.23288
0.80	- 1.1157	0.45716	0.13302
0.90	- 0.80150	0.34121	0.083022
1.00	- 0.57083	0.26650	0.055354
1.20	- 0.25623	0.17884	0.028366
1.40	- 0.052856	0.13086	0.016594
1.60	0.088656	0.10144	0.010631
1.80	0.19235	0.081910	$0.0^{2}72749$
2.00	0.27128	0.068175	$0.0^{2}52325$
2.50	0.40407	0.047196	$0.0^{2}26764$
3.00	0.48544	0.035584	$0.0^{2}15863$
3.50	0.53954	0.028326	$0.0^{2}10350$
4.00	0.57755	0.023407	$0.0^{3}72235$
5.00	0.62618	0.017227	$0.0^{3}40359$
6.00	0.65477	0.013541	$0.0^{3}25479$
8.00	0.68425	$0.0^{2}93956$	$0.0^{3}12640$
10.00	0.69692	$0.0^{2}71479$	$0.0^{4}74727$
15.00	0.70351	$0.0^{2}44262$	$0.0^{4}29739$
25.00	0.69150	$0.0^{2}24789$	$0.0^{5}97889$
50.00	0.65469	$0.0^{2}11621$	$0.0^{5}23129$
100.00	0.60661	$0.0^{3}55671$	$0.0^{6}57609$

Table VIII-C

$-\bar{\eta} = 0{,}03$

T^*	$B^{(2)*}_{Cl}$	$B^{(2)*}_{I}$	$-B^{(2)*}_{II}$
0,30	-10,327	11,328	15,392
0,40	- 4,8058	3,4727	2,9408
0,50	- 2,7862	1,5979	0,94572
0,60	- 1,7842	0,91259	0,40519
0,70	- 1,1966	0,59390	0,20756
0,80	- 0,81409	0,42113	0,11995
0,90	- 0,54686	0,31704	0,075558
1,00	- 0,35041	0,24936	0,050759
1,20	- 0,082297	0,16911	0,026313
1,40	0,090981	0,12468	0,015524
1,60	0,21141	0,097203	0,010011
1,80	0,29950	0,078845	$0,0^{2}68866$
2,00	0,36641	0,065860	$0,0^{2}49745$
2,50	0,47852	0,045891	$0,0^{2}25647$
3,00	0,54672	0,034751	$0,0^{2}15285$
3,50	0,59168	0,027750	$0,0^{2}10014$
4,00	0,62297	0,022985	$0,0^{3}70114$
5,00	0,66237	0,016973	$0,0^{3}39355$
6,00	0,68491	0,013371	$0,0^{3}24926$
8,00	0,70692	$0,0^{2}93039$	$0,0^{3}12419$
10,00	0,71515	$0,0^{2}70904$	$0,0^{4}73620$
15,00	0,71583	$0,0^{2}44010$	$0,0^{4}29414$
25,00	0,69907	$0,0^{2}24697$	$0,0^{5}97158$
50,00	0,65863	$0,0^{2}11596$	$0,0^{5}23027$
100,00	0,60867	$0,0^{3}55604$	$0,0^{6}57457$

Table VIII-D

$-\eta = 0.05$

T^*	$B^{(2)*}_{Cl}$	$B^{(2)*}_{I}$	$-B^{(2)*}_{II}$
0.30	-8.2142	9.2358	12.213
0.40	-3.8109	2.9702	2.4522
0.50	-2.1598	1.4074	0.81305
0.60	-1.3311	0.81995	0.35569
0.70	-0.84238	0.54137	0.18499
0.80	-0.52334	0.38811	0.10816
0.90	-0.30016	0.29471	0.068763
1.00	-0.13605	0.23340	0.046542
1.20	0.08778	0.15996	0.024408
1.40	0.23214	0.11883	0.014523
1.60	0.33219	0.093170	$0.0^{2}9470$
1.80	0.40513	0.075910	$0.0^{2}65188$
2.00	0.46034	0.063636	$0.0^{2}47289$
2.50	0.55222	0.044628	$0.0^{2}24576$
3.00	0.60748	0.033942	$0.0^{2}14728$
3.50	0.64344	0.027188	$0.0^{3}96891$
4.00	0.66809	0.022573	$0.0^{3}68053$
5.00	0.69838	0.016724	$0.0^{3}38376$
6.00	0.71492	0.013203	$0.0^{3}24385$
8.00	0.72952	$0.0^{2}92134$	$0.0^{3}12201$
10.00	0.73332	$0.0^{2}70335$	$0.0^{4}72529$
15.00	0.72812	$0.0^{2}43760$	$0.0^{4}29092$
25.00	0.70663	$0.0^{2}24605$	$0.0^{5}96433$
50.00	0.66257	$0.0^{2}11572$	$0.0^{5}22924$
100.00	0.61073	$0.0^{3}55536$	$0.0^{6}57305$

Table VIII-E

Perfect Gas Contribution

T^*	$B^{(2)*}_{perf}$	T^*	$B^{(2)*}_{perf}$
0,30	0,084435	2,50	0,010132
0,40	0,063326	3,00	$0,0^2 84435$
0,50	0,050661	3,50	$0,0^2 72372$
0,60	0,042217	4,00	$0,0^2 63326$
0,70	0,036186	5,00	$0,0^2 50661$
0,80	0,031663	6,00	$0,0^2 42217$
0,90	0,028145	8,00	$0,0^2 31663$
1,00	0,025330	10,00	$0,0^2 25330$
1,20	0,021109	15,00	$0,0^2 16887$
1,40	0,018093	25,00	$0,0^2 10132$
1,60	0,015832	50,00	$0,0^3 50661$
1,80	0,014072	100,00	$0,0^3 25330$
2,00	0,012665		

APPENDIX II

Table IX

Values of B_{AS}^{II*} for the (9,3),(10,4) and (12,3) models.

T^*	(9,3)	(10,4)	(12,3)
.10	1432.5	2716.0	2458.2
.15	13.870	26.094	23.952
.20	1.0625	1.9750	1.8470
.25	.19721	.36262	0.34476
.30	.058547	.10661	.10287
.35	.023077	.041650	.040726
.40	.010959	.019619	.019417
.45	$.0^2$59274	.010532	.010540
.50	$.0^2$35262	$.0^2$62224	$.0^2$62908
.55	$.0^2$22546	$.0^2$39529	$.0^2$40343
.60	$.0^2$15250	$.0^2$26576	$.0^2$27361
.65	$.0^2$10788	$.0^2$18694	$.0^2$19405
.70	$.0^3$79156	$.0^2$13644	$.0^2$14271
.75	$.0^3$59861	$.0^2$10266	$.0^2$10815
.80	$.0^3$46431	$.0^3$79245	$.0^3$84056
.90	$.0^3$29705	$.0^3$50250	$.0^3$53969
1.00	$.0^3$20268	$.0^3$34011	$.0^3$36940

BIBLIOGRAPHY

1. W.A.Steele and G.D.Halsey, J.Chem.Phys., 22,979 (1954).
2. T.B.MacRury, B.Sc. Thesis, University of British Columbia, Vancouver (1965).
3. J.E.Mayer and M.G.Mayer, "Statistical Mechanics", John Wiley and Sons Inc., N.Y., (1940), Chapter 13.
4. M.P.Freeman and G.D.Halsey, J.Phys.Chem.,59,181 (1955).
5. M.P.Freeman, J.Phys.Chem., 62, 729 (1958).
6. O.Sinanoglu and K.S.Pitzer, J.Chem.Phys., 32, 1279 (1960).
7. J.R. Sams, G. Constabaris, and G.D. Halsey, J.Chem.Phys., 36, 1334 (1962).
8. W.A. Steele, to be published.
9. J.R.Sams, G.Constabaris, and G.D.Halsey, J.Phys.Chem., 64,1689 (1960).
10. R. Yaris, thesis, University of Washington, Seattle, (1962).
11. A.D.McLachlan, Mol.Phys., 7, 387 (1964).
12. R. Wolfe and J.R. Sams, J.Chem.Phys., 44, 2181 (1966).
13. W.C.DeMarcus, E.H.Hopper, and A.M.Allen, U.S. Atomic Energy Commission, KI222 (1955).
14. R.S. Hansen, J.Chem.Phys., 63, 743 (1959).
15. M.P.Freeman, J.Phys.Chem., 64, 32 (1960).
16. G.Constabaris,J.R.Sams, and G.D.Halsey, J.Phys.Chem, 65, 367 (1961).
17. R.P.Bell, Trans.Faraday Soc., 38, 422 (1942).
18. H.F.P.Knaap and J.J.M.Beenakker, Physica, 27, 523 (1961).
19. A.Michels, W. de Graaff, and C.A. Ten Seldam, Physica, 26, 393 (1960).
20. R. Yaris and J.R. Sams, J. Chem.Phys., 37, 571 (1962).

21. G. Uhlenbeck and E.Beth, Physica, 3, 729 (1936).

22. J. De Boer and A. Michels, Physica, 5, 945 (1938).

23. J.O. Hirschfelder, C.F. Curtiss, and R.B.Bird, "Molecular Theory of Gases and Liquids", John Wiley and Sons, N.Y., (1959), Chapter 6.

24. J.R. Sams, Mol. Phys., 9, 17 (1965).

25. J.Kirkwood, Phys. Rev., 44, 31 (1933).

26. J.D.Johnstone and M.L.Klein, Trans.Faraday Soc., 60, 1964 (1964).

27. J.R.Sams, J.Chem.Phys., 43, 2243 (1965).

28. T.L.Hill, "Statistical Mechanics", McGraw-Hill Inc., N.Y., (1959) Chapter 5 and Appendix 10.

29. J.A. Barker and D.H.Everett, Trans.Faraday Soc., 58, 1608 (1962).

30. W.A. Steele and M.Ross, J.Chem.Phys., 35, 850 (1961).

31. J. De Boer, Rep.Prog.Phys., 12, 305 (1949).

32. D. ter Haar, "Elements of Statistical Mechanics", Holt, Rinehart, and Winston, N.Y., (1954), Chapter 8.

33. J.C.Slater, Phys. Rev., 38, 237 (1931).

34. J.C.Slater, J.Chem.Phys., 1, 687 (1933).

35. J.R.Sams, to be published.

36. J.R.Sams, Mol.Phys., 9, 77 (1965).

37. A. Michels and G.W.Nederbragt, Physica, 2, 1000 (1935).

38. G. Thomaes and R.van Steenwinkel, Mol.Phys., 5, 307 (1962).

39. A. Michels and M. Goudeket, Physica, 8, 347 (1941).

40. A. Michels and M. Goudeket, Physica 8, 353 (1941).

41. G. Constabaris, J.R. Sams, and G. Halsey, J.Chem.Phys., 37, 915 (1962).

42. J.G.Kirkwood, Z.Physik, 33, 57 (1932).

43. A.Muller, Proc.Roy.Soc. (London), A154, 624 (1936).

44. K.S. Pitzer, Advances in Chemical Physics Vol. II, Interscience Publishers, Inc., New York (1959), Page 59.

45. H. Margenau, Rev. Modern Phys., 11, 1 (1939).

46. J.P. Olivier and S. Ross, Proc, Roy. Soc. (London), A265, 477(1962).

47. A.L.Myers and J.M.Prausnitz, Trans. Faraday Soc., 61, 755 (1965).